J. Fluid Mech. (1996), *vol.* 319, *pp.* 77–107

Strongly nonlinear vortex–Tollmien–Schlichting-wave interactions in the developing flow through a circular pipe

By A. G. WALTON

Department of Mathematics, Imperial College of Science, Technology and Medicine, 180 Queen's Gate, London SW7 2BZ, UK

(Received 13 November 1995 and in revised form 14 March 1996)

Strongly nonlinear vortex–Tollmien–Schlichting-wave interaction equations are derived for the case where the undisturbed motion represents the developing flow in a circular pipe. The effect upon the equations of moving the wave input position further downstream is investigated and the development of the flow is found to be accelerated by increasing the size of the wave disturbance. Numerical solutions of the three-dimensional interaction equations are presented and indicate that the form of interaction considered here appears to promote the three-dimensionality as the flow develops downstream. It is shown that one of the interactions considered here can develop within an initially two-dimensional Blasius boundary layer.

1. Introduction

Over the past few years a number of studies of the vortex–wave interaction (VWI) equations have been carried out. The main reason for this is that their main property, namely the ability to strongly affect the mean flow in a boundary layer, has obvious applications within the area of laminar–turbulent transition. One possibility is for the waves to be governed predominantly by inviscid effects, in which case the interaction is referred to as a 'vortex–Rayleigh-wave interaction'. In this paper however, we will be concentrating on the situation in which the wave is of viscous–inviscid type, leading to a vortex–Tollmien–Schlichting (TS) interaction. Our aim is to modify the existing works, which have mainly concentrated on external boundary-layers and channel flows (e.g. Hall & Smith 1988, 1991; Smith & Walton 1989; Smith & Blennerhassett 1992) to the case of the developing flow through a pipe of circular cross-section. (In fact, the analysis of § 5 concerning starting solutions for the VWI is also relevant for interactions in external boundary layers.) The weight of theoretical and numerical evidence (e.g. Corcos & Sellars 1959; Gill 1965; Davey & Drazin 1969; Garg & Rouleau 1972) suggests very strongly that the fully-developed flow through such a pipe is stable to both two-dimensional and three-dimensional infinitesimal disturbances, although experiments (e.g. Reynolds 1883; Wygnanski & Champagne 1973) clearly show instability at large Reynolds numbers. Given the ability of the VWI to alter a flow by an $O(1)$ amount, it seems sensible to investigate whether such a process provides a means of explaining the experimental findings. Close to the pipe entrance, the flow is likely to consist of a uniform core of fluid plus a Blasius boundary layer at the wall; thus the natural instability mechanism to consider is that of TS waves. This justifies our decision to concentrate on the vortex–TS interaction although, as remarked by Cowley & Wu (1994), if this interaction leads to the development of an inflexion point in the flow, the

possibility of a vortex–Rayleigh-wave interaction occurring cannot be ruled out. Strong vortex–TS interactions are of two main types, outlined in Hall & Smith (1991), where they are referred to as the 'wide vortex' and 'small vortex'. In fact, the small vortex is also considered in Smith & Walton (1989) where it is called a 'Type III' interaction. The scalings and governing equations for both these interactions are presented in §2.

Throughout the paper the cylindrical polar coordinate system (ax, ar, θ) with origin at the pipe entrance is used, where a represents the pipe radius. The (x, r, θ) velocity components are written $(u, v, w)(F/a^2)$ where F represents the constant flux of fluid through a section of the pipe, the pressure is non-dimensionalized with respect to $\rho(F/a^2)^2$, where ρ is the density of the fluid (assumed incompressible) and the time is written in the form $(a^3/F)t$. We define the global Reynolds number

$$R = F/a\nu, \tag{1.1}$$

which we assume throughout to be asymptotically large. The three-dimensional unsteady Navier–Stokes equations can then be written in the non-dimensional form

$$\frac{\partial u}{\partial x}+\frac{\partial v}{\partial r}+\frac{v}{r}+\frac{1}{r}\frac{\partial w}{\partial \theta}=0, \tag{1.2a}$$

$$\frac{\partial u}{\partial t}+u\frac{\partial u}{\partial x}+v\frac{\partial u}{\partial r}+\frac{w}{r}\frac{\partial u}{\partial \theta}=-\frac{\partial p}{\partial x}+\frac{1}{R}\left(\frac{\partial^2 u}{\partial x^2}+\frac{\partial^2 u}{\partial r^2}+\frac{1}{r}\frac{\partial u}{\partial r}+\frac{1}{r^2}\frac{\partial^2 u}{\partial \theta^2}\right), \tag{1.2b}$$

$$\frac{\partial v}{\partial t}+u\frac{\partial v}{\partial x}+v\frac{\partial v}{\partial r}+\frac{w}{r}\frac{\partial v}{\partial \theta}-\frac{w^2}{r}=-\frac{\partial p}{\partial r}+\frac{1}{R}\left(\frac{\partial^2 v}{\partial x^2}+\frac{\partial^2 v}{\partial r^2}+\frac{1}{r}\frac{\partial v}{\partial r}+\frac{1}{r^2}\frac{\partial^2 v}{\partial \theta^2}-\frac{v}{r^2}-\frac{2}{r^2}\frac{\partial w}{\partial \theta}\right), \tag{1.2c}$$

$$\frac{\partial w}{\partial t}+u\frac{\partial w}{\partial x}+v\frac{\partial w}{\partial r}+\frac{w}{r}\frac{\partial w}{\partial \theta}+\frac{vw}{r}=-\frac{1}{r}\frac{\partial p}{\partial \theta}+\frac{1}{R}\left(\frac{\partial^2 w}{\partial x^2}+\frac{\partial^2 w}{\partial r^2}+\frac{1}{r}\frac{\partial w}{\partial r}+\frac{1}{r^2}\frac{\partial^2 w}{\partial \theta^2}-\frac{w}{r^2}+\frac{2}{r^2}\frac{\partial v}{\partial \theta}\right), \tag{1.2d}$$

and are subject to the usual no-slip boundary conditions at the wall $r = 1$, supplemented by regularity conditions along the pipe axis $r = 0$.

The structure of the remainder of the paper is as follows. Section 2 concerns the derivation of the 'wide vortex' interaction equations. We supply a little more detail than has been presented in previous papers on the subject in an attempt to provide the reader with an understanding of the processes involved, in particular how such a large effect can be generated owing to the difference in lengthscales between the mean flow and the three-dimensional TS wave. In §3 the interaction equations are formulated for the particular case of the developing flow through a circular pipe. It is found that there is a crucial distance downstream of the entrance at which the VWI is influenced by the effects of curvature. Further downstream at a distance of $O(R)$ from the entrance, the lengthscales of the mean flow and wave become comparable and viscous and inertial effects become equally important across the entire pipe cross-section. In §4 we concentrate on the 'small vortex' interaction in which only a sublayer of the boundary layer is affected significantly by the interaction. This interaction arises from a larger input disturbance than the wide vortex, and as a consequence the development of the flow is accelerated, with the lengthscales of the mean flow and wave coinciding before the $O(R)$ distance at which inertial and viscous effects fill the pipe. In this situation the VWI develops into a form of triple-deck interaction. A numerical scheme is developed to solve the resulting interaction equations and numerical results are presented. Section 5 concerns the question of whether the wide vortex interaction can be initiated from realistic starting conditions. Clearly if this is not the case, the usefulness of the

interaction is rather limited. Here we consider the case where a three-dimensional TS wave is introduced into a two-dimensional Blasius boundary-layer at various positions downstream of the entrance and in each case deduce the initial development of the interaction. Finally, in §6 conclusions are drawn and areas of further research proposed.

2. Derivation of the interaction equations

In Hall & Smith (1991), the scalings were given for the so-called wide vortex– and small vortex–TS interactions for the case of an external boundary-layer flow. The aim of the present work is to demonstrate how the form of the two different vortex–wave interactions changes with distance from the pipe entrance. At first the interaction proceeds in an analogous fashion to the external case, then curvature effects come into play and eventually the wave and mean flow lengthscales become comparable. The distances downstream at which these alterations occur depend on the input disturbance size. Not surprisingly, the larger the disturbance the further upstream these adjustments take place. We start by considering the wide vortex–TS interaction. Readers familiar with the scalings for this interaction are directed to §3 were the application to internal flows is discussed. In this section, we present a thorough derivation of the scalings and governing equations, going into more detail than is found in Hall & Smith (1991). Once the scalings in the various regions have been established for this interaction, it is straightforward to generalize these to the small vortex–TS interaction which we discuss later. For the following discussion concerning the behaviour near the entrance of the pipe it is convenient to define a local Reynolds number

$$Re = R\hat{L}, \tag{2.1}$$

where $\hat{L}$ denotes distance along the pipe, with $\hat{L} = 0$ at the pipe entrance.

In the wide vortex–TS interaction, the aim is to alter the streamwise mean flow by an $O(1)$ amount throughout the entire boundary layer which has the classical thickness $Re^{-1/2}\hat{L}$. The standard three-dimensional triple-deck framework is used to describe the effect of the TS wave on the mean flow. Thus, in addition to the boundary layer or main deck, we have a sublayer where viscous and inertial effects are equally important of $O(Re^{-5/8}\hat{L})$ thickness (the lower deck) and an outer region of linearized potential flow with $O(Re^{-3/8}\hat{L})$ thickness (the upper deck). The wave dependence is expressed in the form

$$E \equiv \exp(\mathrm{i}\alpha X - \mathrm{i}\Omega T), \tag{2.2}$$

where $X = Re^{3/8}\hat{L}^{-1}x$, $T = Re^{1/4}\hat{L}^{-1}t$ are the short streamwise lengthscale and timescale associated with the wave and the azimuthal lengthscale is of $O(Re^{-3/8}\hat{L})$. The scalings quoted here can be found in Smith (1979*a*) and many subsequent high-Reynolds-number studies involving TS waves. A key idea is that the wave remains neutral throughout the interaction so that the wavenumber α and frequency Ω are both real quantities and are allowed to vary on the lengthscales and timescales associated with the mean flow. We now explain how to deduce the rest of the scalings involved in the wide vortex–TS interaction. Our aim is to determine the size of TS disturbance necessary to provoke an $O(1)$ streamwise flow within the boundary layer. This flow is required to develop over the same lengthscale as that associated with the boundary layer, namely $O(\hat{L})$. We suppose the unknown flow to be three-dimensional, a consequence of which is that the $\partial u/\partial x$ and $\partial w/\partial\theta$ terms in the continuity equation (1.2*a*) must be comparable in size. Assuming that there is only one lengthscale in the

θ-direction, namely the $O(Re^{-3/8}\hat{L})$ scale associated with the three-dimensional TS wave, and balancing the aforementioned terms in the continuity equation, we see that the required azimuthal mean flow is of $O(Re^{-3/8})$. In view of the smallness of this quantity it might be suspected that only a tiny wave disturbance is necessary to generate this flow, and this proves to be the case. This is the basic principle underlying this and other vortex–wave interactions. In order to see how this azimuthal flow is induced, we turn to the lower deck of the triple-deck structure, where the normal variable $y \sim Re^{-5/8}\hat{L}$, and the waves are driven by the unknown shear flow (equations 2.11(a–c) below). In turn, the waves drive the mean-flow correction via an inertial–viscous balance (see equations (2.14a–c)). If δ denotes the size of the azimuthal component of the wave (with δ to be determined), then the size of the azimuthal mean flow component w_m is deduced from the balance between $(w\,\partial w/\partial\theta)_{wave}$ and $Re^{-1}\hat{L}\,\partial^2 w_m/\partial y^2$ in (1.2d). This gives:

$$Re^{3/8}\hat{L}^{-1}\delta^2 \sim (Re^{-1}\hat{L})(Re^{-5/8}\hat{L})^{-2}w_m \Rightarrow w_m = O(Re^{1/8}\delta^2). \tag{2.3}$$

We will see below (equation (2.13c)) that the azimuthal wave velocity decays like $1/Y$ as $Y \to \infty$, where Y represents the scaled lower deck coordinate, leading to logarithmic growth of w_m. Thus upon reaching the matching region between the lower deck and the boundary layer (where Y is of $O(Re^{1/8})$) the azimuthal mean flow has grown to $O(Re^{1/8}\delta^2 \ln Re^{1/8})$. Setting this quantity equal to the desired magnitude of $O(Re^{-3/8})$, we have

$$Re^{1/8}\delta^2 \ln Re^{1/8} \sim Re^{-3/8},$$

implying a wave amplitude δ of magnitude

$$\delta = \frac{Re^{-1/4}}{(\ln Re^{1/8})^{1/2}}. \tag{2.4}$$

Thus, in particular

$$w_m = \frac{Re^{-3/8}}{\ln Re^{1/8}}w_{20}, \quad w_{wave} = \frac{Re^{-1/4}}{(\ln Re^{1/8})^{1/2}}w_{11}E + \text{c.c.},$$

with w_{20}, w_{11} of $O(1)$ and c.c. denoting complex conjugate. Now that δ has been determined, it is a straightforward matter to determine the rest of the scalings involved in the interaction. The appropriate multi-scalings in x and t are:

$$\frac{\partial}{\partial x} = Re^{3/8}\hat{L}^{-1}\frac{\partial}{\partial X} + \hat{L}^{-1}\frac{\partial}{\partial \bar{x}}, \quad \frac{\partial}{\partial t} = Re^{1/4}\hat{L}^{-1}\frac{\partial}{\partial T} + \hat{L}^{-1}\frac{\partial}{\partial \bar{t}}, \tag{2.5a,b}$$

where in each case the first term describes the 'fast' wave response and the second represents the scale associated with the induced mean flow. As explained above, the azimuthal scaling is

$$\frac{\partial}{\partial \theta} = Re^{3/8}\hat{L}^{-1}\frac{\partial}{\partial \bar{\theta}}, \tag{2.6}$$

and in view of the form of δ in (2.4) we define the large parameter

$$M \equiv (\ln Re^{1/8})^{1/2}. \tag{2.7}$$

Motivated by the order of magnitude arguments discussed above we now set out the flow expansions in the three decks and then derive the governing equations for the wide vortex–TS interaction near the pipe entrance.

(i) Lower deck ($r = 1 - Re^{-5/8}\hat{L}Y$):

$$u = Re^{-1/8}\lambda Y + \ldots + \frac{Re^{-1/4}}{M}(u_{11}E + \text{c.c.}) + \ldots + \frac{Re^{-3/8}}{M^2}(u_{20} + u_{22}E^2 + \text{c.c.}) + \ldots, \quad (2.8a)$$

$$v = -\frac{Re^{-1/2}}{M}(v_{11}E + \text{c.c.}) - \frac{Re^{-5/8}}{M^2}(v_{20} + v_{22}E^2 + \text{c.c.}) + \ldots, \quad (2.8b)$$

$$w = \frac{Re^{-1/4}}{M}(w_{11}E + \text{c.c.}) + \frac{Re^{-3/8}}{M^2}(w_{20} + w_{22}E^2 + \text{c.c.}) + \ldots, \quad (2.8c)$$

$$p = -\tfrac{1}{2}U_e^2 + \ldots + \frac{Re^{-3/8}}{M}(p_{11}E + \text{c.c.}) + \ldots. \quad (2.8d)$$

(ii) Main deck ($r = 1 - Re^{-1/2}\hat{L}\bar{Y}$):

$$u = U_0 + \ldots + \frac{Re^{-1/4}}{M}\left(A_{11}\frac{\partial U_0}{\partial \bar{Y}}E + \text{c.c.}\right) + \ldots, \quad (2.9a)$$

$$v = \frac{Re^{-3/8}}{M}(\mathrm{i}\alpha A_{11}U_0 E + \text{c.c.}) - Re^{-1/2}V_0 + \ldots, \quad (2.9b)$$

$$w = Re^{-3/8}W_0 + \frac{Re^{-3/8}}{M}(w_w E + \text{c.c.}) + \ldots, \quad (2.9c)$$

$$p = -\tfrac{1}{2}U_e^2 + \ldots + \frac{Re^{-3/8}}{M}(p_{11}E + \text{c.c.}) + \ldots. \quad (2.9d)$$

(iii) Upper deck ($r = 1 - Re^{-3/8}\hat{L}\bar{\bar{y}}$):

$$u = U_e + \ldots + \frac{Re^{-3/8}}{M}(\bar{\bar{u}}E + \text{c.c.}) + \ldots, \quad (2.10a)$$

$$v = -Re^{-3/8}U_e'(\bar{x})\bar{\bar{y}} + \ldots + \frac{Re^{-3/8}}{M}(\bar{\bar{v}}E + \text{c.c.}) + \ldots, \quad (2.10b)$$

$$w = \frac{Re^{-3/8}}{M}(\bar{\bar{w}}E + \text{c.c.}) + \ldots, \quad (2.10c)$$

$$p = -\tfrac{1}{2}U_e^2 + \ldots + \frac{Re^{-3/8}}{M}(\bar{\bar{p}}E + \text{c.c.}) + \ldots. \quad (2.10d)$$

Substituting these expansions into the Navier–Stokes equations we obtain the governing interaction equations. We start with the lower deck where the TS wave is driven by the unknown induced shear flow λY where $\lambda = \lambda(\bar{\theta}, \bar{x}, \bar{t})$. Substitution of (2.8) into (1.2) leads to the following wave balances:

$$\mathrm{i}\alpha u_{11} + \frac{\partial v_{11}}{\partial Y} + \frac{\partial w_{11}}{\partial \bar{\theta}} = 0, \quad (2.11a)$$

$$-\mathrm{i}\Omega u_{11} + \mathrm{i}\alpha\lambda Y u_{11} + \lambda v_{11} + \frac{\partial \lambda}{\partial \bar{\theta}}Y w_{11} = -\mathrm{i}\alpha p_{11} + \frac{\partial^2 u_{11}}{\partial Y^2}, \quad (2.11b)$$

$$\frac{\partial p_{11}}{\partial Y} = 0, \quad -\mathrm{i}\Omega w_{11} + \mathrm{i}\alpha\lambda Y w_{11} = -\frac{\partial p_{11}}{\partial \bar{\theta}} + \frac{\partial^2 w_{11}}{\partial Y^2}, \quad (2.11c)$$

subject to the no-slip boundary conditions

$$u_{11} = v_{11} = w_{11} = 0 \quad \text{on} \quad Y = 0, \tag{2.11d}$$

with matching conditions to the main deck

$$u_{11} \to \lambda A_{11}, \quad w_{11} \to 0 \quad \text{as} \quad Y \to \infty, \tag{2.11e,f}$$

where A_{11} is the wave contribution to the boundary-layer displacement. In conventional linear stability analyses λ is constant; however, even with λ dependent on $\bar{\theta}$, it is possible to reduce the system (2.11) to an equation describing the evolution of the wave pressure p_{11} (for details see Smith 1979*b*). The equation takes the form

$$\left.\begin{aligned} &\frac{\partial^2 p_{11}}{\partial \bar{\theta}^2} - \frac{1}{\lambda}\frac{\partial \lambda}{\partial \bar{\theta}}\mathscr{F}(\xi)\frac{\partial p_{11}}{\partial \bar{\theta}} - \alpha^2 p_{11} = (\mathrm{i}\alpha\lambda)^{5/3}\frac{\mathrm{Ai}'(\xi)}{\kappa(\xi)}A_{11}, \\ &\text{where} \\ &\mathscr{F}(\xi) = \tfrac{3}{2} + \frac{\xi}{2\,\mathrm{Ai}(\xi)}(\xi\kappa(\xi) + \mathrm{Ai}'(\xi)), \quad \xi = -\frac{\mathrm{i}^{1/3}\Omega}{(\alpha\lambda)^{2/3}}, \quad \kappa(\xi) = \int_{\xi}^{\infty} \mathrm{Ai}(s)\,\mathrm{d}s, \end{aligned}\right\} \tag{2.12}$$

and Ai denotes the Airy function. It can be seen that the mean flow affects the wave in a nonlinear fashion via the occurrence of both λ and ξ in this equation. If there is no interaction and λ is a constant, this equation reduces to the familiar linear stability eigenrelation for TS waves. To confirm the statements made above concerning the growth of the azimuthal mean flow it is necessary to determine the asymptotic behaviour of the wave components in the lower deck. From (2.11) we deduce that as $Y \to \infty$:

$$u_{11} \sim \lambda A_{11} - \left[\frac{1}{\alpha^2}\frac{\partial}{\partial \bar{\theta}}\left(\frac{1}{\lambda}\frac{\partial p_{11}}{\partial \bar{\theta}}\right)\right]\frac{1}{Y} + O\left(\frac{1}{Y^2}\right), \tag{2.13a}$$

$$v_{11} \sim -\mathrm{i}\alpha\lambda A_{11}\, Y + \left[-\frac{\mathrm{i}\alpha p_{11}}{\lambda} + \frac{1}{\mathrm{i}\alpha\lambda^2}\frac{\partial\lambda}{\partial\bar{\theta}}\frac{\partial p_{11}}{\partial\bar{\theta}} + \frac{\mathrm{i}}{\alpha}\frac{\partial}{\partial\bar{\theta}}\left(\frac{1}{\lambda}\frac{\partial p_{11}}{\partial\bar{\theta}}\right) + \mathrm{i}\Omega A_{11}\right] + O\left(\frac{1}{Y}\right), \tag{2.13b}$$

$$w_{11} \sim -\left[\frac{1}{\mathrm{i}\alpha\lambda}\frac{\partial p_{11}}{\partial\bar{\theta}}\right]\frac{1}{Y} + \left[\frac{\mathrm{i}\Omega}{\alpha^2\lambda^2}\frac{\partial p_{11}}{\partial\bar{\theta}}\right]\left(\frac{1}{Y^2}\right) + O\left(\frac{1}{Y^3}\right). \tag{2.13c}$$

Once again from substitution of the lower deck expansions (2.8) into (1.2), the induced mean flow is found to satisfy

$$\frac{\partial v_{20}}{\partial Y} + \frac{\partial w_{20}}{\partial \bar{\theta}} = 0, \tag{2.14a}$$

$$\lambda v_{20} + w_{20}\, Y\frac{\partial\lambda}{\partial\bar{\theta}} + \left[v_{11}\frac{\partial u_{11}^*}{\partial Y} + w_{11}\frac{\partial u_{11}^*}{\partial\bar{\theta}} + \text{c.c.}\right] = \frac{\partial^2 u_{20}}{\partial Y^2}, \tag{2.14b}$$

$$\left[\mathrm{i}\alpha u_{11}^* w_{11} + v_{11}\frac{\partial w_{11}^*}{\partial Y} + w_{11}\frac{\partial w_{11}^*}{\partial\bar{\theta}} + \text{c.c.}\right] = \frac{\partial^2 w_{20}}{\partial Y^2}, \tag{2.14c}$$

with * denoting complex conjugate. Using (2.13) and (2.14) it is possible to deduce the asymptotic form of the mean terms as $Y \to \infty$. We find $u_{20} \propto Y^3 \ln Y$, $v_{20} \propto Y \ln Y$ and

$$w_{20} \sim -q \ln Y \quad \text{as} \quad Y \to \infty,$$

where

$$q = \frac{1}{\alpha^2 \lambda^2} \frac{\partial}{\partial \bar{\theta}} \left\{ \alpha^2 p_{11} p_{11}^* + \frac{\partial p_{11}}{\partial \bar{\theta}} \frac{\partial p_{11}^*}{\partial \bar{\theta}} \right\}. \tag{2.15}$$

This confirms the claims made just below (2.3). Note that it is only the mean term that undergoes this logarithmic growth; the analogous equations to (2.14*b*, *c*) for u_{22}, w_{22} contain the additional terms $i\alpha\lambda Y u_{22}$, $i\alpha\lambda Y w_{22}$, respectively: these serve to inhibit the growth of the higher harmonics. At first sight, another possibility appears to be for w_{20} to grow like Y as $Y \to \infty$ from (2.14c). This leads to an overspecified problem in the main deck, however, and so need not be considered further.

Next we turn to the equations in the man deck or boundary layer. We have anticipated the expressions for the wave in the expansions (2.9) for u and v: these can be verified by substitution of (2.9) into (1.2). This process also reveals that the mean part of the flow satisfies the unsteady three-dimensional boundary-layer equations

$$\frac{\partial U_0}{\partial \bar{x}} + \frac{\partial V_0}{\partial \bar{Y}} + \frac{\partial W_0}{\partial \bar{\theta}} = 0, \tag{2.16*a*}$$

$$\frac{\partial U_0}{\partial \bar{t}} + U_0 \frac{\partial U_0}{\partial \bar{x}} + V_0 \frac{\partial U_0}{\partial \bar{Y}} + W_0 \frac{\partial U_0}{\partial \bar{\theta}} = U_e U_e'(\bar{x}) + \frac{\partial^2 U_0}{\partial \bar{Y}^2}, \tag{2.16*b*}$$

$$\frac{\partial W_0}{\partial \bar{t}} + U_0 \frac{\partial W_0}{\partial \bar{x}} + V_0 \frac{\partial W_0}{\partial \bar{Y}} + W_0 \frac{\partial W_0}{\partial \bar{\theta}} = \frac{\partial^2 W_0}{\partial \bar{Y}^2}, \tag{2.16*c*}$$

with matching conditions to the lower deck:

$$U_0 = V_0 = 0, \quad W_0 = -q \quad \text{on} \quad \bar{Y} = 0, \tag{2.16*d*, *e*}$$

$$\lambda = \partial U_0 / \partial \bar{Y} \quad \text{on} \quad \bar{Y} = 0. \tag{2.16*f*}$$

As in the conventional triple-deck TS framework, the upper deck is a region of linearized potential flow and the appropriate matching conditions from the main deck are:

$$U_0 \to U_e(\bar{x}), \quad W_0 \to 0 \quad \text{as} \quad \bar{Y} \to \infty, \tag{2.17}$$

where $U_e(\bar{x})$ represents the external slip velocity arising from the outer inviscid flow. In order to close the system of governing equations we require a relation associating the wave pressure p_{11} with the wave contribution to the boundary-layer displacement A_{11}. This is found by substituting the upper-deck expansions (2.10) into (1.2), and leads to the pressure equation

$$\left(\frac{\partial^2}{\partial \bar{y}^2} + \frac{\partial^2}{\partial \bar{\theta}^2} - \alpha^2 \right) \bar{p} = 0, \tag{2.18}$$

subject to the matching conditions

$$\partial \bar{p} / \partial \bar{y} = -\alpha^2 A_{11}, \quad \bar{p} = p_{11} \quad \text{on} \quad \bar{y} = 0,$$

to ensure, respectively, continuity of normal velocity and pressure. The solution to (2.18) is also required to decay in the far field.

Thus the governing system for the wide vortex TS interaction reduces to solving (2.16) for the mean flow in the boundary layer with q given by (2.15) and p_{11} by (2.12). In general, the governing equations require a numerical solution and their strongly nonlinear nature renders such a task non-trivial. To the author's knowledge there has only been one attempt at a numerical solution of the full governing equations, namely that of Hall & Smith (1991). In that paper, the starting conditions imposed assume that

the flow is already three-dimensional, with the spanwise component required to satisfy a compatibility condition. For a particular three-dimensional input, Hall & Smith's calculations terminated in an apparent finite-distance singularity, although it is possible that the singularity is purely numerical. Later, in §5, we investigate the development of the interaction from an initially two-dimensional Blasius boundary layer. We turn now to the question of how the interaction equations are modified further downstream of the pipe entrance.

3. The effect of curvature on the wide vortex–TS interaction

The system of interaction equations was derived in §2 for a location near the entrance to the pipe. In this situation the equations are precisely the same as if the flow were unconfined. We might expect that as we move down the pipe, i.e. increase $\hat{L}$, the effects of confinement and curvature must eventually play a significant role in the interaction. The explicit $\hat{L}$-dependence in the scalings (2.5)–(2.10) is deceptive because in addition Re is dependent on $\hat{L}$. Thus, in what follows, we work in terms of the global Reynolds number R $(= Re/\hat{L})$. For convenience we define a scaled downstream distance

$$L = \epsilon^3 \hat{L} \quad \text{where} \quad \epsilon \equiv R^{-1/5} \ll 1. \tag{3.1}$$

The situation envisaged is one in which the flow enters the pipe at $\hat{L} = 0$ with a uniform velocity profile $u = 1$. In order that a constant flux of fluid is maintained, the flow at the centre of the pipe must accelerate in view of the retarding effect of viscosity at the wall. Since the boundary layer is of thickness $O(\epsilon L^{1/2})$ in terms of the new parameters, there is a correction to the uniform core flow of the same magnitude. Thus the core flow expands in the form

$$U_e(\bar{x}) = 1 + \epsilon L^{1/2} U_{e1}(\bar{x}) + \ldots, \tag{3.2}$$

with a similar expansion for the mean contribution to the pressure. We will now rewrite the scalings (2.5)–(2.10) in terms of the new parameters ϵ and L, rather than Re and $\hat{L}$. The multi-scalings have the form

$$\frac{\partial}{\partial x} = L^{-5/8}\frac{\partial}{\partial X} + \epsilon^3 L^{-1}\frac{\partial}{\partial \bar{x}}, \quad \frac{\partial}{\partial t} = \epsilon L^{-3/4}\frac{\partial}{\partial T} + \epsilon^3 L^{-1}\frac{\partial}{\partial \bar{t}}, \tag{3.3a, b}$$

$$\frac{\partial}{\partial \theta} = L^{-5/8}\frac{\partial}{\partial \bar{\theta}}, \quad M \equiv (-\ln(\epsilon L^{-1/8}))^{1/2}, \tag{3.3c, d}$$

and the expansions in the three asymptotic regions are as follows:

(i) lower deck $(r = 1 - \epsilon^2 L^{3/8} Y)$:

$$u = \epsilon L^{-1/8}\lambda Y + \ldots + \frac{\epsilon^2 L^{-1/4}}{M}(u_{11}E + \text{c.c.}) + \ldots + \frac{\epsilon^3 L^{-3/8}}{M^2}(u_{20} + u_{22}E^2 + \text{c.c.}) + \ldots, \tag{3.4a}$$

$$v = -\frac{\epsilon^4 L^{-1/2}}{M}(v_{11}E + \text{c.c.}) - \frac{\epsilon^5 L^{-5/8}}{M^2}(v_{20} + v_{22}E^2 + \text{c.c.}) + \ldots, \tag{3.4b}$$

$$w = \frac{\epsilon^2 L^{-1/4}}{M}(w_{11}E + \text{c.c.}) + \frac{\epsilon^3 L^{-3/8}}{M^2}(w_{20} + w_{22}E^2 + \text{c.c.}) + \ldots, \tag{3.4c}$$

$$p = \epsilon L^{1/2}\bar{P}(\bar{x}) + \ldots + \frac{\epsilon^3 L^{-3/8}}{M}(p_{11}E + \text{c.c.}) + \ldots; \tag{3.4d}$$

(ii) main deck ($r = 1-\epsilon L^{1/2}\bar{Y}$):

$$u = U_0 + \ldots + \frac{\epsilon^2 L^{-1/4}}{M}\left(A_{11}\frac{\partial U_0}{\partial \bar{Y}}E + \text{c.c.}\right) + \ldots, \tag{3.5a}$$

$$v = \frac{\epsilon^3 L^{-3/8}}{M}(\mathrm{i}\alpha A_{11} U_0 E + \text{c.c.}) - \epsilon^4 L^{-1/2} V_0 + \ldots, \tag{3.5b}$$

$$w = \epsilon^3 L^{-3/8} W_0 + \frac{\epsilon^3 L^{-3/8}}{M}(w_w E + \text{c.c.}) + \ldots, \tag{3.5c}$$

$$p = \epsilon L^{1/2}\bar{P}(\bar{x}) + \ldots + \frac{\epsilon^3 L^{-3/8}}{M}(p_{11} E + \text{c.c.}) + \ldots; \tag{3.5d}$$

(iii) upper deck ($r = 1-L^{5/8}\bar{y}$):

$$u = 1 + \epsilon L^{1/2} U_{e1}(\bar{x}) + \ldots + \frac{\epsilon^3 L^{-3/8}}{M}(\bar{u}E + \text{c.c.}) + \ldots, \tag{3.6a}$$

$$v = \frac{\epsilon^3 L^{-3/8}}{M}(\bar{v}E + \text{c.c.}) + \ldots, \tag{3.6b}$$

$$w = \frac{\epsilon^3 L^{-3/8}}{M}(\bar{w}E + \text{c.c.}) + \ldots, \tag{3.6c}$$

$$p = \epsilon L^{1/2}\bar{P}(\bar{x}) + \ldots + \frac{\epsilon^3 L^{-3/8}}{M}(\bar{p}E + \text{c.c.}) + \ldots. \tag{3.6d}$$

Since we have not altered the scalings in any way, the governing equations remain as before except for the removal of the term $U_e U_e'(\bar{x})$ from the right-hand side of (2.16*b*) and the replacement of U_e by unity in (2.17). These equations remain valid provided $\hat{L} < R^{3/5}$, and we shall henceforth refer to this as region I of the pipe. The first effects of curvature appear at distances of $O(R^{3/5})$, when L is $O(1)$. This result was first deduced by Smith & Bodonyi (1980) in their weakly nonlinear study of the stability of developing pipe flow to three-dimensional TS waves. At such distances, the upper deck extends across the entire cross-section of the pipe and the azimuthal scaling increases to $O(1)$. Thus, the effects of confinement and curvature impress themselves upon the flow. In order to investigate the development of this interaction further downstream ($L \geqslant O(1)$) we must seek new scalings with respect to L. First, when $L = O(1)$, the governing interaction equations are

$$\frac{\partial U_0}{\partial \bar{x}} + \frac{\partial V_0}{\partial \bar{Y}} + \frac{\partial W_0}{\partial \bar{\theta}} = 0, \tag{3.7a}$$

$$\frac{\partial U_0}{\partial \bar{t}} + U_0\frac{\partial U_0}{\partial \bar{x}} + V_0\frac{\partial U_0}{\partial \bar{Y}} + W_0\frac{\partial U_0}{\partial \bar{\theta}} = \frac{\partial^2 U_0}{\partial \bar{Y}^2}, \tag{3.7b}$$

$$\frac{\partial W_0}{\partial \bar{t}} + U_0\frac{\partial W_0}{\partial \bar{x}} + V_0\frac{\partial W_0}{\partial \bar{Y}} + W_0\frac{\partial W_0}{\partial \bar{\theta}} = \frac{\partial^2 W_0}{\partial \bar{Y}^2}, \tag{3.7c}$$

subject to

$$U_0 = V_0 = 0, \quad W_0 = -q \quad \text{on} \quad \bar{Y} = 0, \tag{3.7d}$$

$$U_0 \to 1, \quad W_0 \to 0 \quad \text{as} \quad \bar{Y} \to \infty, \tag{3.7e}$$

$$q = \frac{1}{\alpha^2\lambda^2}\frac{\partial}{\partial \bar{\theta}}\left\{\underline{\alpha^2 p_{11} p_{11}^*} + \frac{\partial p_{11}}{\partial \bar{\theta}}\frac{\partial p_{11}^*}{\partial \bar{\theta}}\right\}, \tag{3.7f}$$

with p_{11} found from the solution of

$$\frac{\partial^2 p_{11}}{\partial \bar{\theta}^2} - \frac{1}{\lambda}\frac{\partial \lambda}{\partial \bar{\theta}}\mathscr{F}(\xi)\frac{\partial p_{11}}{\partial \bar{\theta}} \underline{\underline{-\alpha^2 p_{11}}} = (\mathrm{i}\alpha\lambda)^{5/3}\frac{\mathrm{Ai}'(\xi)}{\kappa(\xi)}A_{11}; \quad \lambda = \left.\frac{\partial U_0}{\partial \bar{Y}}\right|_{\bar{Y}=0}, \tag{3.7g}$$

$$\left(\frac{\partial^2}{\partial r^2} + \frac{1}{r}\frac{\partial}{\partial r} + \frac{1}{r^2}\frac{\partial^2}{\partial \bar{\theta}^2} \underline{\underline{-\alpha^2}}\right)\bar{\bar{p}} = 0, \quad \partial\bar{\bar{p}}/\partial r = \alpha^2 A_{11}, \quad \bar{\bar{p}} = p_{11} \quad \text{on} \quad r = 1. \tag{3.7h}$$

The reason for underlining certain terms will be made clear later. We see that the only alteration to the governing equations which were valid for $L < O(1)$ is in the upper deck (compare (2.18) with (3.7h)). The region of validity of (3.7), i.e. $L \sim O(1)$, will be referred to as region IIa. A clue to the appropriate scalings for $L > O(1)$ arises from the linearized TS stability analysis performed by Smith & Bodonyi (1980), part of which we repeat here. Provided the streamwise flow U_0 remains $O(1)$, the balancing of terms in (3.7b) indicates that the unknown skin-friction λ scales with $\bar{x}^{-1/2}$. For example, if the mean flow within the boundary layer is the classical Blasius flow at leading order, then $U_0 = f'_B(\bar{Y}/\bar{x}^{1/2})$ and $\lambda = \hat{\lambda}/\bar{x}^{1/2}$ where $\hat{\lambda} \simeq 0.33205$. With this value for λ and setting $p_{11} \propto \cos N\theta$, (3.7$g$, h) combine to yield the linear stability eigenrelation

$$-N^2 - \alpha^2 = \frac{(\mathrm{i}\alpha\hat{\lambda})^{5/3}}{\bar{x}^{5/6}}\frac{\mathrm{Ai}'(\xi)}{\kappa(\xi)}\frac{I'_N(\alpha)}{\alpha I_N(\alpha)}, \tag{3.8}$$

where I_N is the Nth-order modified Bessel function of the first kind. For neutral stability (i.e. α real), the eigenrelation becomes:

$$N^2 + \alpha^2 \simeq 1.000\,65\alpha^{2/3}\frac{I'_N(\alpha)}{I_N(\alpha)}\hat{\lambda}^{5/3}\bar{x}^{-5/6}. \tag{3.9}$$

Using the asymptotic form $I'_N(\alpha)/I_N(\alpha) \sim N/\alpha$ as $\alpha \to 0$ we see that

$$\alpha \propto \bar{x}^{-5/2} \quad \text{as} \quad \bar{x} \to \infty. \tag{3.10}$$

In addition, for ξ in (2.12) to remain $O(1)$, the frequency Ω must scale as $(\alpha\lambda)^{2/3} \sim \bar{x}^{-2}$. These results suggest the streamwise and temporal multi-scalings

$$\frac{\partial}{\partial x} = L^{-5/2}\frac{\partial}{\partial X} + \epsilon^3 L^{-1}\frac{\partial}{\partial \bar{x}}, \quad \frac{\partial}{\partial t} = \epsilon L^{-2}\frac{\partial}{\partial T} + \epsilon^3 L^{-1}\frac{\partial}{\partial \bar{t}}, \tag{3.11}$$

for the region $O(1) < L < O(\epsilon^{-2})$, which we shall henceforth refer to as region IIb. We note that when $L \sim O(\epsilon^{-2})$, i.e. an $O(R)$ distance downstream, the wave and mean flow scalings become comparable. We investigate this further presently. In view of the property $I'_N(\alpha)/I_N(\alpha) \to 1$ as $\alpha \to \infty$, the eigenrelation (3.9) implies that $\alpha \propto \bar{x}^{-5/8}$ as $\bar{x} \to 0$, in agreement with the scaling in region I. Thus, region IIa can be regarded as a thin adjustment region in which the flow sheds its external properties and develops internal characteristics. The azimuthal scaling in region IIb is $O(1)$, i.e.

$$\frac{\partial}{\partial \theta} = \frac{\partial}{\partial \bar{\theta}}, \tag{3.12}$$

and the rest of the scalings are chosen so that the resulting governing equations are changed as little as possible from those governing the interaction in region I, i.e. equations (3.7). After some trial and error the appropriate expansions for region IIb can be shown to be:

(i) lower deck ($r = 1-\epsilon^2 LY$):

$$u = \epsilon L^{1/2}\lambda Y + \frac{\epsilon^2 L}{M}(u_{11}E + \text{c.c.}) + \frac{\epsilon^3 L^{3/2}}{M^2}(u_{20} + u_{22}E^2 + \text{c.c.}) + \ldots, \tag{3.13a}$$

$$v = -\frac{\epsilon^4 L^{-1/2}}{M}(v_{11}E + \text{c.c.}) - \frac{\epsilon^5}{M^2}(v_{20} + v_{22}E^2 + \text{c.c.}) + \ldots, \tag{3.13b}$$

$$w = \frac{\epsilon^2 L^{-3/2}}{M}(w_{11}E + \text{c.c.}) + \frac{\epsilon^3 L^{-1}}{M^2}(w_{20} + w_{22}E^2 + \text{c.c.}) + \ldots, \tag{3.13c}$$

$$p = \epsilon L^{1/2}\bar{P}(\bar{x}) + \ldots + \frac{\epsilon^3 L^{-7/2}}{M}(p_{11}E + \text{c.c.}) + \ldots; \tag{3.13d}$$

(ii) main deck ($r = 1-\epsilon L^{1/2}\bar{Y}$):

$$u = U_0 + \ldots + \frac{\epsilon^2 L}{M}\left(A_{11}\frac{\partial U_0}{\partial \bar{Y}}E + \text{c.c.}\right) + \ldots, \tag{3.14a}$$

$$v = \frac{\epsilon^3 L^{-1}}{M}(\mathrm{i}\alpha A_{11}U_0 E + \text{c.c.}) - \epsilon^4 L^{-1/2}V_0 + \ldots, \tag{3.14b}$$

$$w = \epsilon^3 L^{-1}W_0 + \frac{\epsilon^3 L^{-1}}{M}(w_w E + \text{c.c.}) + \ldots, \tag{3.14c}$$

$$p = \epsilon L^{1/2}\bar{P}(\bar{x}) + \ldots + \frac{\epsilon^3 L^{-7/2}}{M}(p_{11}E + \text{c.c.}) + \ldots; \tag{3.14d}$$

(iii) upper deck ($r = O(1)$):

$$u = 1 + \epsilon L^{1/2}U_{e1}(\bar{x}) + \ldots + \frac{\epsilon^3 L^{-7/2}}{M}(\bar{u}E + \text{c.c.}) + \ldots, \tag{3.15a}$$

$$v = \frac{\epsilon^3 L^{-1}}{M}(\bar{v}E + \text{c.c.}) + \ldots, \tag{3.15b}$$

$$w = \frac{\epsilon^3 L^{-1}}{M}(\bar{w}E + \text{c.c.}) + \ldots, \tag{3.15c}$$

$$p = \epsilon L^{1/2}\bar{P}(\bar{x}) + \ldots + \frac{\epsilon^3 L^{-7/2}}{M}(\bar{p}E + \text{c.c.}) + \ldots, \tag{3.15d}$$

where the large parameter M is now given by

$$M \equiv (-\ln(L^{1/2}\epsilon))^{1/2}. \tag{3.16}$$

Note that the above scalings coincide with those in Region I (i.e. (3.3)–(3.6)) when L is $O(1)$. It should be stressed that the proposed form of evolution of the flow from region I to region II is not the only possibility. For instance for certain starting conditions the flow in region I may terminate in a finite distance singularity (Hall & Smith 1991). Substitution of the scalings (3.11)–(3.16) into the Navier–Stokes equations (1.2) and working as before, we find that the governing equations are as in region II*a*, i.e. (3.7), but without the underlined terms. Such terms might be expected to lose their importance as we move downstream since the effective wavenumber is decreasing, as may be inferred from (3.10), for example.

Eventually, when $L \sim O(\epsilon^{-2})$, the wave and vortex lengthscales and timescales become comparable, both of $O(R)$. At such distances all three layers extend across the whole of the pipe with the flow predominantly in the streamwise direction. Setting $L = O(\epsilon^{-2})$ in the above scalings the scalings in the 'fully-developed' region III are

$$\frac{\partial}{\partial x} = R^{-1}\frac{\partial}{\partial \bar{x}}, \quad \frac{\partial}{\partial t} = R^{-1}\frac{\partial}{\partial \bar{t}}, \quad \frac{\partial}{\partial \theta} = \frac{\partial}{\partial \bar{\theta}}, \tag{3.17}$$

with the flow expanding in the form

$$u = U_0 + \ldots, \tag{3.18a}$$

$$v = R^{-1} V_0 + \ldots, \tag{3.18b}$$

$$w = R^{-1} W_0 + \ldots, \tag{3.18c}$$

$$p = \bar{P}(\bar{x}) + R^{-2} P_0 + \ldots \tag{3.18d}$$

with (U_0, V_0, W_0, P_0) all dependent on $(\bar{x}, r, \bar{\theta}, \bar{t})$. Substitution of the above expansions into the N–S equations yields

$$\frac{\partial U_0}{\partial \bar{x}} + \frac{\partial V_0}{\partial r} + \frac{V_0}{r} + \frac{1}{r}\frac{\partial W_0}{\partial \bar{\theta}} = 0, \tag{3.19a}$$

$$\frac{\partial U_0}{\partial \bar{t}} + U_0\frac{\partial U_0}{\partial \bar{x}} + V_0\frac{\partial U_0}{\partial r} + \frac{W_0}{r}\frac{\partial U_0}{\partial \bar{\theta}} = -\bar{P}'(\bar{x}) + \frac{\partial^2 U_0}{\partial r^2} + \frac{1}{r}\frac{\partial U_0}{\partial r} + \frac{1}{r^2}\frac{\partial^2 U_0}{\partial \bar{\theta}^2}, \tag{3.19b}$$

$$\frac{\partial V_0}{\partial \bar{t}} + U_0\frac{\partial V_0}{\partial \bar{x}} + V_0\frac{\partial V_0}{\partial r} + \frac{W_0}{r}\frac{\partial V_0}{\partial \bar{\theta}} - \frac{W_0^2}{r} = -\frac{\partial P_0}{\partial r} + \frac{\partial^2 V_0}{\partial r^2} + \frac{1}{r}\frac{\partial V_0}{\partial r} + \frac{1}{r^2}\frac{\partial^2 V_0}{\partial \bar{\theta}^2} - \frac{V_0}{r^2} - \frac{2}{r^2}\frac{\partial W_0}{\partial \bar{\theta}}, \tag{3.19c}$$

$$\frac{\partial W_0}{\partial \bar{t}} + U_0\frac{\partial W_0}{\partial \bar{x}} + V_0\frac{\partial W_0}{\partial r} + \frac{W_0}{r}\frac{\partial W_0}{\partial \bar{\theta}} + \frac{V_0 W_0}{r} = -\frac{1}{r}\frac{\partial P_0}{\partial \bar{\theta}} + \frac{\partial^2 W_0}{\partial r^2} + \frac{1}{r}\frac{\partial W_0}{\partial r} + \frac{1}{r^2}\frac{\partial^2 W_0}{\partial \bar{\theta}^2} - \frac{W_0}{r^2} + \frac{2}{r^2}\frac{\partial V_0}{\partial \bar{\theta}}. \tag{3.19d}$$

The relevant boundary conditions are

$$U_0 = V_0 = W_0 = 0 \quad \text{on} \quad r = 1,$$

to ensure no slip, with regularity conditions along the pipe axis $r = 0$. In addition the pressure term $\bar{P}$ is determined by the condition of constant mass flux through the pipe, or from maintaining a constant pressure gradient as is perhaps more often the case in experiments. We see from (3.19) that the flow is governed by almost the full Navier–Stokes equations with the exception of the $\partial^2/\partial x^2$ terms which have lost their importance owing to the long lengthscale over which the flow is now developing. One solution of this system is the unidirectional parabolic profile $U_0 = 1 - r^2$, $\bar{P}'(\bar{x})$ constant (Hagen–Poiseuille flow or HPF). Several authors (see Crabtree, Küchemann & Sowerby 1963 and references therein) have examined the development from a uniform entry flow to the Poiseuille profile, and matched the two solutions together numerically, but there seems no *a priori* reason why the parabolic profile should be attained downstream and in experiments this is not usually the case unless great care is taken to control the disturbance environment. We note that (3.19) is parabolic in $\bar{x}$, so that no downstream conditions can be imposed here. Computations of (3.19) from uniform

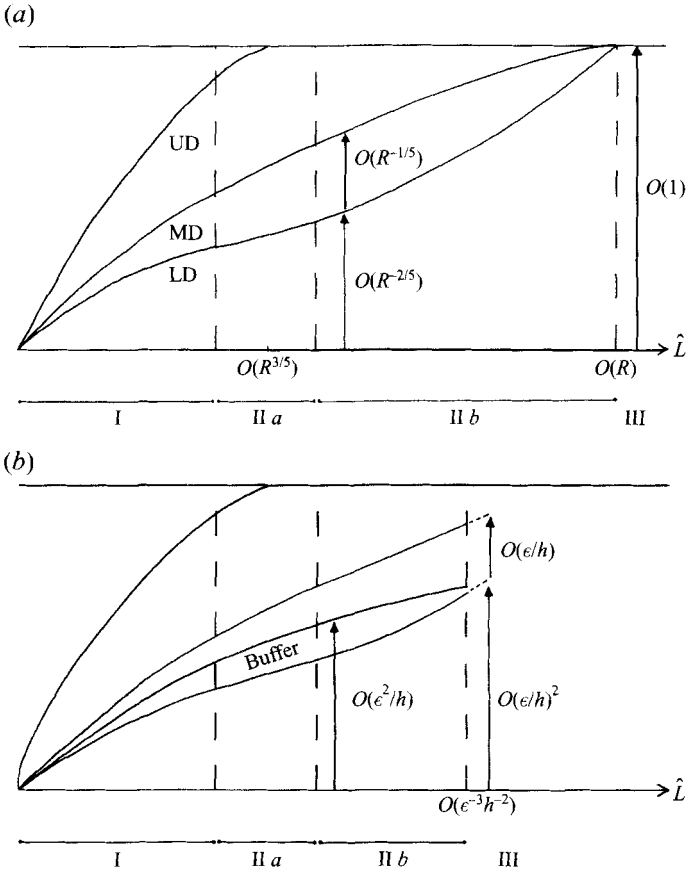

FIGURE 1. The development of the structure of (*a*) the wide vortex, (*b*) the small vortex, as the position of wave input $\hat{L}$ is increased.

entry conditions with $\partial/\partial\bar{x} \equiv 0$ and $\bar{P}'(\bar{x})$ fixed were carried out in Walton (1991). In this situation the HPF profile is reached rapidly in time. It would be interesting to see if this is also the case for the marching version of (3.19) and for cases in which the mass flux rather than the pressure gradient is fixed.

To summarize, we have shown how the wide vortex interaction equations alter as the location L of wave input is moved downstream; the scalings derived enable L to be scaled out of the equations in each of the regions I, II*a* and II*b*. A diagrammatical summary of the different stages of development is given in figure 1 (*a*). We return to the wide vortex in §5, where the initial linear development of the interaction in the regions I, II*a* and II*b* from a two-dimensional boundary layer is considered. In the next section we derive the scalings and governing equations for the small vortex.

4. The small vortex–TS interaction

4.1. *Scalings and governing equations*

We will now attempt to motivate the scalings for the so-called small vortex–TS interaction given in Hall & Smith (1991), Smith & Walton (1989). The aim of this interaction is to alter the flow completely in a sublayer of the boundary layer of relative thickness $O(\epsilon/h)$ where $O(\epsilon) < h < O(1)$. We will follow Hall & Smith's terminology

and refer to this sublayer as the 'buffer region', although in other works the term 'diffusion layer' is often used. The case of $h \sim O(\epsilon)$ is the wide vortex discussed in §§2 and 3, while if $h \sim O(1)$, the nonlinear effects are confined to the lower deck (i.e. we have a conventional triple-deck problem). It is useful to regard h as a measure of the size of the TS disturbance. For definiteness, we suppose that the flow in the remainder of the boundary layer or main deck is of the Blasius form. Since this flow is proportional to the boundary-layer coordinate close to the wall, the undisturbed streamwise flow will be of order ϵ/h within the buffer region. For a strong interaction we require the induced flow to be of the same magnitude. In view of the viscous–inertial balance operating within this layer, the flow must vary over a lengthscale x deduced from equating the sizes of the terms $u\partial u/\partial x$ and $R^{-1}\partial^2 u/\partial y^2$ in (1.2b) where $u \sim \epsilon/h$ and $y \sim (\epsilon/h)\epsilon L^{1/2}$ with L defined as in §3. This gives $x = h^{-3}L\tilde{x}$, say, with $\tilde{x}$ of $O(1)$. Thus, the induced flow now varies over a shorter lengthscale than the $O(\epsilon^{-3}L)$ scale associated with the Blasius flow. As expected, when $h \sim O(\epsilon)$, the two lengthscales become comparable. These order-of-magnitude arguments suggest that the appropriate streamwise multi-scaling for the small vortex is

$$\frac{\partial}{\partial x} = L^{-5/8}\frac{\partial}{\partial \bar{X}} + h^3 L^{-1}\frac{\partial}{\partial \tilde{x}} + \epsilon^3 L^{-1}\frac{\partial}{\partial \bar{x}}, \tag{4.1}$$

(cf. (3.3)) with the wave lengthscale remaining as in the wide vortex case. If, in addition, the induced flow is time-dependent, the appropriate temporal multi-scaling has the form

$$\frac{\partial}{\partial t} = \epsilon\left(L^{-3/4}\frac{\partial}{\partial \bar{T}} + h^2 L^{-1}\frac{\partial}{\partial \tilde{t}}\right). \tag{4.2}$$

The scaling for the azimuthal variable θ is as previously, namely

$$\frac{\partial}{\partial \theta} = L^{-5/8}\frac{\partial}{\partial \bar{\theta}}, \tag{4.3}$$

while the large parameter M is now dependent on h rather than ϵ and takes the form

$$M \equiv (-\ln(hL^{-1/8}))^{1/2}, \tag{4.4}$$

(cf. 3.3d). All these scaling reduce to their wide vortex counterparts as $h \to O(\epsilon)$. It is a straightforward matter now to generalize the wide vortex expansions of region I to the small vortex case. We omit the details of the expansions in the four flow regions but remark that the relevant scalings with respect to the Reynolds number are now those of the triple-deck for pipe entry flow (Smith & Bodonyi 1980). This means that the governing equations for the small vortex can be derived from either the triple-deck equations or the full Navier–Stokes equations, in contrast to the wide vortex–TS interaction. Proceeding as in §3, we find that the governing equations for the mean flow within the buffer region are

$$\frac{\partial U_0}{\partial \tilde{x}} + \frac{\partial V_0}{\partial \tilde{Y}} + \frac{\partial W_0}{\partial \bar{\theta}} = 0, \tag{4.5a}$$

$$\frac{\partial U_0}{\partial \tilde{t}} + U_0\frac{\partial U_0}{\partial \tilde{x}} + V_0\frac{\partial U_0}{\partial \tilde{Y}} + W_0\frac{\partial U_0}{\partial \bar{\theta}} = \frac{\partial^2 U_0}{\partial \tilde{Y}^2}, \tag{4.5b}$$

$$\frac{\partial W_0}{\partial \tilde{t}} + U_0\frac{\partial W_0}{\partial \tilde{x}} + V_0\frac{\partial W_0}{\partial \tilde{Y}} + W_0\frac{\partial W_0}{\partial \bar{\theta}} = \frac{\partial^2 W_0}{\partial \tilde{Y}^2}, \tag{4.5c}$$

with

$$U_0 = V_0 = 0, \quad W_0 = -q \quad \text{on} \quad \tilde{Y} = 0, \quad U_0 \sim \hat{\lambda}\bar{x}^{-1/2}(\tilde{Y} + A_0), \quad W_0 \to 0 \quad \text{as} \quad \tilde{Y} \to \infty, \tag{4.5d}$$

$$q = \frac{1}{\alpha^2\lambda^2}\frac{\partial}{\partial\bar{\theta}}\left\{\underline{\alpha^2 p_{11} p_{11}^*} + \frac{\partial p_{11}}{\partial\bar{\theta}}\frac{\partial p_{11}^*}{\partial\bar{\theta}}\right\}, \tag{4.5e}$$

$$\frac{\partial^2 p_{11}}{\partial\bar{\theta}^2} - \frac{1}{\lambda}\frac{\partial\lambda}{\partial\bar{\theta}}\mathscr{F}(\xi)\frac{\partial p_{11}}{\partial\bar{\theta}} - \underline{\alpha^2 p_{11}} = (\mathrm{i}\alpha\lambda)^{5/3}\frac{\mathrm{Ai}'(\xi)}{\kappa(\xi)}A_{11}; \quad \lambda = \left.\frac{\partial U_0}{\partial\bar{Y}}\right|_{\tilde{Y}=0}, \tag{4.5f}$$

$$\left(\frac{\partial^2}{\partial\bar{y}^2} + \frac{\partial^2}{\partial\bar{\theta}^2} - \alpha^2\right)\bar{p} = 0, \tag{4.5g}$$

$$\partial\bar{p}/\partial\bar{y} = -\alpha^2 A_{11}, \quad \bar{p} = p_{11} \quad \text{on} \quad \bar{y} = 0.$$

It is evident that, apart from notational changes, the only alteration from the wide vortex case is in the outer boundary condition on U_0 in (4.5*d*). Intuitively, it may seem surprising that increasing the disturbance size from $O(\epsilon)$ to $O(h)$ leads to a narrower region in which the flow is modified. However, we can see from the order of magnitude arguments above that the flow in the thinner layer develops over a shorter lengthscale, and therefore a larger disturbance is required to accelerate the development. Further downstream, for L of $O(1)$, i.e. $\hat{L} \sim O(\epsilon^{-3})$, a new region is entered (cf. region II*a* for the wide vortex) where the effects of curvature become important. As in the wide vortex case, the only alteration to the governing equations is that (4.5*g*) is replaced by

$$\left(\frac{\partial^2}{\partial r^2} + \frac{1}{r}\frac{\partial}{\partial r} + \frac{1}{r^2}\frac{\partial^2}{\partial\bar{\theta}^2} - \alpha^2\right)\bar{p} = 0, \quad \partial\bar{p}/\partial r = \alpha^2 A_{11}, \quad \bar{p} = p_{11} \quad \text{on} \quad r = 1. \tag{4.6}$$

We can generalize the arguments of §3 concerning the further downstream development for $\hat{L} > O(\epsilon^{-3})$ to the small vortex case. If the flow in the buffer region remains of a Blasius nature at leading order, then the linear neutral stability eigenrelation (3.9) (which is still valid for the small vortex case) yields $\alpha \propto \bar{x}^{-5/2}$, since $\lambda \propto \bar{x}^{-1/2}$. Arguing as before, the multi-scalings for the downstream region II*b* where $O(1) < L < O(h^{-2})$, can then be set out as follows:

$$\left.\begin{aligned} \frac{\partial}{\partial x} &= L^{-5/2}\frac{\partial}{\partial X} + h^3 L^{-1}\frac{\partial}{\partial\tilde{x}} + \epsilon^3 L^{-1}\frac{\partial}{\partial\bar{x}}, \quad \frac{\partial}{\partial t} = \epsilon\left(L^{-2}\frac{\partial}{\partial T} + h^2 L^{-1}\frac{\partial}{\partial\tilde{t}}\right), \\ \frac{\partial}{\partial\theta} &= \frac{\partial}{\partial\bar{\theta}}, \quad M \equiv (-\ln(L^{1/2}h))^{1/2} \gg 1. \end{aligned}\right\} \tag{4.7}$$

The governing equations in the buffer layer remain as in (4.5) and (4.6) but as for the wide vortex, the terms underlined in (4.5*e*,*f*) and (4.6) are no longer present. We note that it is possible for the small vortex to develop in a different way to that anticipated here: for example, the mean flow in the buffer region may acquire a similarity solution (Walton & Smith 1992). To the author's knowledge, no marching computations of the small vortex–TS system have yet been attempted, so the likelihood of achieving the similarity solution downstream is unknown. In any case, for a primarily two-dimensional starting condition the development suggested here would seem more likely. The initial linear development from such a starting condition is investigated in §5 for the wide vortex case.

As for the wide vortex, the vortex and wave lengthscales eventually become comparable as L increases. However, with the enhanced disturbance size this occurs closer to the entrance than the $O(R)$ distance associated with the development of the Blasius boundary layer, specifically when $L \sim O(h^{-2})$ or $\hat{L} \sim O(\epsilon^{-3}h^{-2})$. At this streamwise location, the buffer region and lower deck merge together and the parameter M decreases to $O(1)$. Thus, the flow acquires a three-tier structure. With the wave and vortex lengthscales comparable, the multi-scalings in region III are

$$\frac{\partial}{\partial x} = h^5 \frac{\partial}{\partial \tilde{x}} + \epsilon^3 h^2 \frac{\partial}{\partial \bar{x}}, \quad \frac{\partial}{\partial t} = \epsilon h^4 \frac{\partial}{\partial \tilde{t}}, \quad \frac{\partial}{\partial \theta} = \frac{\partial}{\partial \bar{\theta}}. \tag{4.8}$$

The flow expansions can be deduced directly from the scalings of region IIb and take the form:

(i) lower deck ($r = 1-(\epsilon/h)^2 \tilde{Y}$):

$$u = \epsilon h^{-1} U + \ldots, \tag{4.9a}$$

$$v = -\epsilon^3 h^2 V + \ldots, \tag{4.9b}$$

$$w = \epsilon h^4 W + \ldots, \tag{4.9c}$$

$$p = \epsilon h^{-1} \bar{P}(\bar{x}) + \ldots + \epsilon^2 h^8 P + \ldots; \tag{4.9d}$$

(ii) main deck ($r = 1-(\epsilon/h)\bar{Y}$):

$$u = U_B(\bar{Y}/\bar{x}^{1/2}) + \epsilon h^{-1} A U_B' + \ldots, \tag{4.10a}$$

$$v = \epsilon^2 h^3 (\partial A/\partial \bar{x})\, U_B + \ldots, \tag{4.10b}$$

$$w = \epsilon^2 h^3 w_m + \ldots, \tag{4.10c}$$

$$p = \epsilon h^{-1} \bar{P}(\bar{x}) + \ldots + \epsilon^2 h^8 P + \ldots; \tag{4.10d}$$

(iii) upper deck (r of $O(1)$):

$$u = 1 + \epsilon h^{-1} U_{e1}(\bar{x}) + \ldots + \epsilon^2 h^8 \bar{\bar{u}} + \ldots, \tag{4.11a}$$

$$v = \epsilon^2 h^3 \bar{\bar{v}} + \ldots, \tag{4.11b}$$

$$w = \epsilon^2 h^3 \bar{\bar{w}} + \ldots, \tag{4.11c}$$

$$p = \epsilon h^{-1} \bar{P}(\bar{x}) + \ldots + \epsilon^2 h^8 \bar{\bar{p}} + \ldots. \tag{4.11d}$$

Substitution into the Navier–Stokes equations (1.2) reveals the flow to be governed by the interactive boundary-layer equations

$$\frac{\partial U}{\partial \tilde{x}} + \frac{\partial V}{\partial \tilde{Y}} + \frac{\partial W}{\partial \bar{\theta}} = 0, \tag{4.12a}$$

$$\frac{\partial U}{\partial \tilde{t}} + U\frac{\partial U}{\partial \tilde{x}} + V\frac{\partial U}{\partial \tilde{Y}} + W\frac{\partial U}{\partial \bar{\theta}} = \frac{\partial^2 U}{\partial \tilde{Y}^2}, \tag{4.12b}$$

$$\frac{\partial W}{\partial \tilde{t}} + U\frac{\partial W}{\partial \tilde{x}} + V\frac{\partial W}{\partial \tilde{Y}} + W\frac{\partial W}{\partial \bar{\theta}} = -\frac{\partial P}{\partial \bar{\theta}} + \frac{\partial^2 W}{\partial \tilde{Y}^2}, \tag{4.12c}$$

subject to

$$U = V = W = 0 \quad \text{on} \quad \tilde{Y} = 0, \quad U \sim \hat{\lambda} \bar{x}^{-1/2}(\tilde{Y} + A), \quad W \to 0 \quad \text{as} \quad \tilde{Y} \to \infty, \tag{4.12d}$$

with the pressure P linked to the displacement A via the solution of the system

$$\left(\frac{\partial^2}{\partial r^2}+\frac{1}{r}\frac{\partial}{\partial r}+\frac{1}{r^2}\frac{\partial^2}{\partial \bar{\theta}^2}\right)\bar{p}=0, \quad \bar{p}=P, \quad \partial\bar{p}/\partial r=-\partial^2 A/\partial \tilde{x}^2 \quad \text{on} \quad r=1. \quad (4.12e)$$

Finite time and distance singularity structures have been proposed for similar three-dimensional systems by Hoyle & Smith (1994). F. T. Smith (personal communication) has expressed the view that with regard to (4.12), a singularity may arise in the azimuthal direction, given the form of the pressure–displacement relation (4.12*e*). Certainly, the development of such singularities in the system could be of relevance to pipe-flow transition; we consider the numerical solution of this triple-deck problem in the next subsection. A summary of the various stages of development of the small vortex interaction is presented in figure 1(*b*).

4.2. *The numerical solution of the triple-deck problem*

4.2.1. *The numerical scheme*

In order to investigate how the interaction evolves downstream it is necessary to solve (4.12) numerically. We restrict ourselves here to the steady case, mainly because of the expense and complexity of computing the time-dependent flow. In order to capture the periodicity of the motion, the velocity components and the pressure are written in Fourier series form. For example, the streamwise velocity component is written

$$U=U_0(\tilde{x},\tilde{Y})+\sum_{n=1}^{N}U_n(\tilde{x},\tilde{Y})\,\mathrm{e}^{\mathrm{i}n\theta}+\text{c.c.} \quad (4.13)$$

The choice of truncation number N is discussed later. These expansions are substituted into (4.12), yielding $2N+1$ nonlinear differential equations (first order in $\tilde{x}$, second order in $\tilde{Y}$) for each of the unknowns U_n, W_n and their complex conjugates. In particular the azimuthal components W_n satisfy equations of the form

$$\begin{aligned}\frac{\partial^2 W_n}{\partial \tilde{Y}^2}=&\,\mathrm{i}nP_n+\mathrm{i}n\,W_0\,W_n+V_0\frac{\partial W_n}{\partial \tilde{Y}}+V_n\frac{\partial W_0}{\partial \tilde{Y}}+U_0\frac{\partial W_n}{\partial \tilde{x}}+U_n\frac{\partial W_0}{\partial \tilde{x}}\\&+\sum_{k=1}^{n-1}\mathrm{i}(n-k)\,W_k\,W_{n-k}+V_k\frac{\partial W_{n-k}}{\partial \tilde{Y}}+U_k\frac{\partial W_{n-k}}{\partial \tilde{x}}\\&+\sum_{k=n+1}^{N}\mathrm{i}(n-k)\,W_k\,W^*_{k-n}+V_k\frac{\partial W^*_{k-n}}{\partial \tilde{Y}}+U_k\frac{\partial W^*_{k-n}}{\partial \tilde{x}}\\&+\sum_{k=1}^{N-n}\mathrm{i}(n+k)\,W^*_k\,W_{n+k}+V^*_k\frac{\partial W_{n+k}}{\partial \tilde{Y}}+U^*_k\frac{\partial W_{n+k}}{\partial \tilde{x}},\end{aligned} \quad (4.14)$$

for $n=1,\ldots,N$, where * denotes complex conjugate. The main difference between this equation and that satisfied by U_n is in the appearance of the pressure P_n in the former, which is linked to U_n via the relation

$$nP_n=-\frac{\partial^2 U_n}{\partial \tilde{x}^2}(\tilde{x},\infty), \quad (4.15)$$

stemming from the solution of (4.12*e*).

The bulk of the computation consists of solving the momentum and continuity equations using a finite-difference scheme of second-order accuracy in both $\tilde{x}$ and $\tilde{Y}$.

Derivatives with respect to $\tilde{Y}$ are represented by standard central difference formulae, while $\tilde{x}$-derivatives are written in the form

$$\frac{\partial f_k^{m+1}}{\partial \tilde{x}} = (\tfrac{3}{2}f_k^{m+1} - 2f_k^m + \tfrac{1}{2}f_k^{m-1})/\Delta x, \tag{4.16}$$

with the superscript denoting x-location. For more details see Fletcher (1991). In order to implement this scheme a one-level algorithm is necessary to commence the downstream march, i.e. when $m = 1$. Thus, at the beginning of the computation we employ a first-order accurate method in $\tilde{x}$, obtaining overall second-order accuracy by means of Richardson extrapolation. This method is used for the first two x-steps of the march. An additional complication arises from the pressure–velocity relation (4.15). For the first two steps the pressure is calculated using the central-difference representation:

$$nP_n^{m+1} = -(U_{n,\infty}^{m+2} - 2U_{n,\infty}^{m+1} + U_{n,\infty}^{m})/(\Delta x)^2, \tag{4.17}$$

in which $U_{n,\infty}^{m+2} (n = 1, \ldots, N)$ are unknown at step $m+1$. To overcome this problem, guesses are made for these quantities enabling W_n to be calculated from the discretized version of (4.14). U_n^{m+2} is then calculated from the $\tilde{x}$-momentum equation, leading to new estimates for $U_{n,\infty}^{m+2}$. The process is repeated until convergence is obtained. Typically, less than 10 iterations were required before successive iterates differed by less than 10^{-8}.

If it were necessary to perform this iteration at each downstream location, the computation would be extremely expensive. Once two steps have been computed, however, it is possible to replace (4.17) by the asymmetric second-order formula

$$nP_n^{m+1} = -(2U_{n,\infty}^{m+1} - 5U_{n,\infty}^{m} + 4U_{n,\infty}^{m-1} - U_{n,\infty}^{m-2})/(\Delta x)^2, \tag{4.18}$$

in which the right-hand side is known once U_n^{m+1} is computed from the $\tilde{x}$-momentum equation. From this stage onwards it is possible to use the second-order accurate marching scheme to compute the downstream evolution without recourse to any further iteration. This speeds up the computation considerably. At each $\tilde{x}$-step a block tridiagonal system of equations is obtained, and these are solved efficiently using the Thomas algorithm.

4.2.2. *Starting conditions*

Computations were performed for both the interactive and non-interactive ($P \equiv 0$ in (4.12*c*)) versions of (4.12). In order to obtain suitable starting conditions for both cases, we adopt the following approach. Writing

$$U = \tilde{Y} + \epsilon \tilde{x}^{1/3} \tilde{u}(\eta) \cos\theta, \tag{4.19a}$$

$$V = \epsilon \tilde{x}^{-1/3} \tilde{v}(\eta) \cos\theta, \tag{4.19b}$$

$$W = \epsilon \tilde{x}^{-2/3} \tilde{w}(\eta) \sin\theta, \tag{4.19c}$$

$$P = \epsilon \tilde{x}^{-5/3} \tilde{p} \cos\theta, \tag{4.19d}$$

where $\eta = \tilde{Y}/\tilde{x}^{1/3}$, $\epsilon \ll 1$ and substituting into (4.12), we obtain the equations

$$\tfrac{1}{3}\tilde{u} - \tfrac{1}{3}\eta\tilde{u}' + \tilde{v}' + \tilde{w} = 0, \tag{4.20a}$$

$$\tfrac{1}{3}\eta\tilde{u} - \tfrac{1}{3}\eta^2\tilde{u}' + \tilde{v} = \tilde{u}'', \quad -\tfrac{2}{3}\eta\tilde{w} - \tfrac{1}{3}\eta^2\tilde{w}' = \tfrac{2}{3}\tilde{x}^{-1/3}\tilde{A} + \tilde{w}'', \tag{4.20b, c}$$

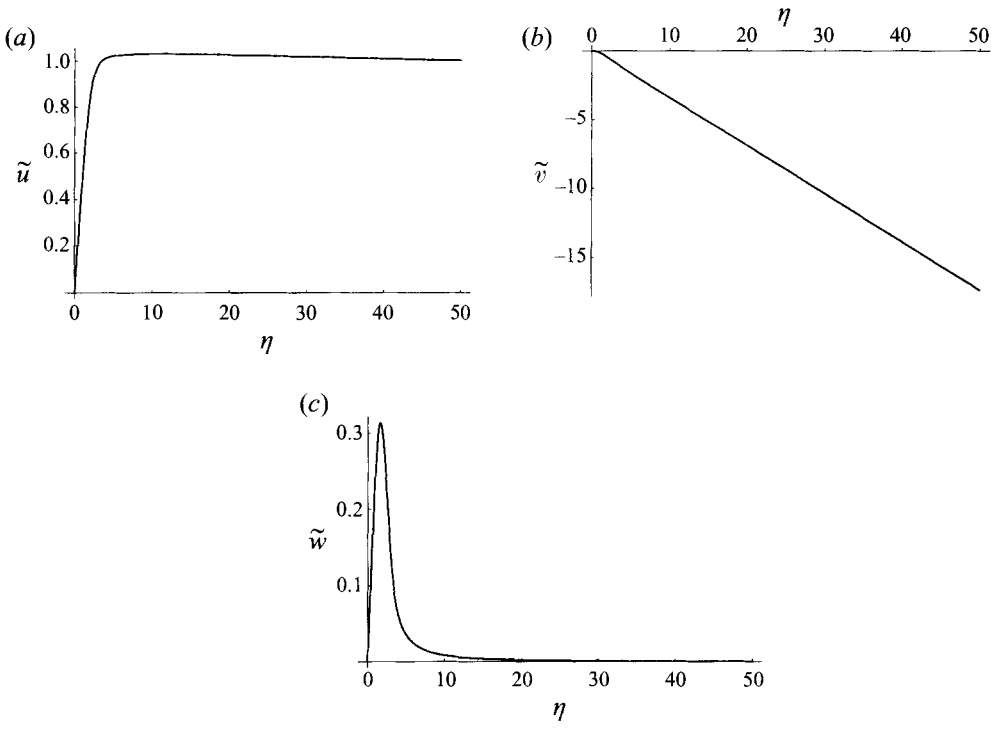

FIGURE 2. (*a*) The streamwise velocity component $\tilde{u}(\eta)$, (*b*) the normal velocity component $\tilde{v}(\eta)$, (*c*) the azimuthal velocity component $\tilde{w}(\eta)$, calculated from the numerical solution of the non-interactive version of (4.20).

with $\tilde{u} = \tilde{v} = \tilde{w} = 0$ on $\eta = 0$ and $\tilde{u} \to \tilde{A}$, $\tilde{w} \to 0$ as $\eta \to \infty$. For the non-interactive case we use, as our starting profile at $\tilde{x} = 1$, the numerical solution of (4.20) with $\tilde{A} \equiv 0$ on the right-hand side of (4.20*c*). In the interactive situation $\tilde{A}$ is normalized to unity and the system is solved with $\tilde{x} = 1$ in (4.20c). The velocity profiles for the two cases are shown in figures 2 and 3.

4.2.3. *Numerical results*

Plots of velocity components arising from the numerical solution of (4.12) are shown in figures 4 and 5 for the non-interactive and interactive cases, respectively. All the results are for an initial disturbance size $\epsilon = 0.01$. In the former case (figure 4) the solution appears to retain the self-similar form (4.19), activity thereby being confined mainly to the first mode. Since higher modes are negligible, plots of these quantities are not presented here. The results shown are for computations performed using $\Delta x = 0.01$, $\Delta y = 0.05$, $N = 4$ with the value of $\tilde{Y}_\infty$ taken to be 50. The large value of this final parameter here and in the interactive case is necessary because the decay as $\tilde{Y} \to \infty$ of the azimuthal component of the starting solution is only algebraic in nature (see figures 2(*c*), 3(*c*)). The non-interactive numerical results appear to be relatively insensitive to further refinement in $\tilde{x}$ and $\tilde{Y}$. Turning now to the interactive case, higher modes are excited within only a few $\tilde{x}$-steps of the starting location. Figure 5 shows how the interaction develops between $\tilde{x} = 1$ and $\tilde{x} = 1.14$, for the parameter values $\mathrm{d}x = 0.01$, $\mathrm{d}y = 0.05$, $\tilde{Y}_\infty = 50$ and truncation number $N = 8$. Beyond this position in $\tilde{x}$ more Fourier modes are required to describe the solution accurately and this is

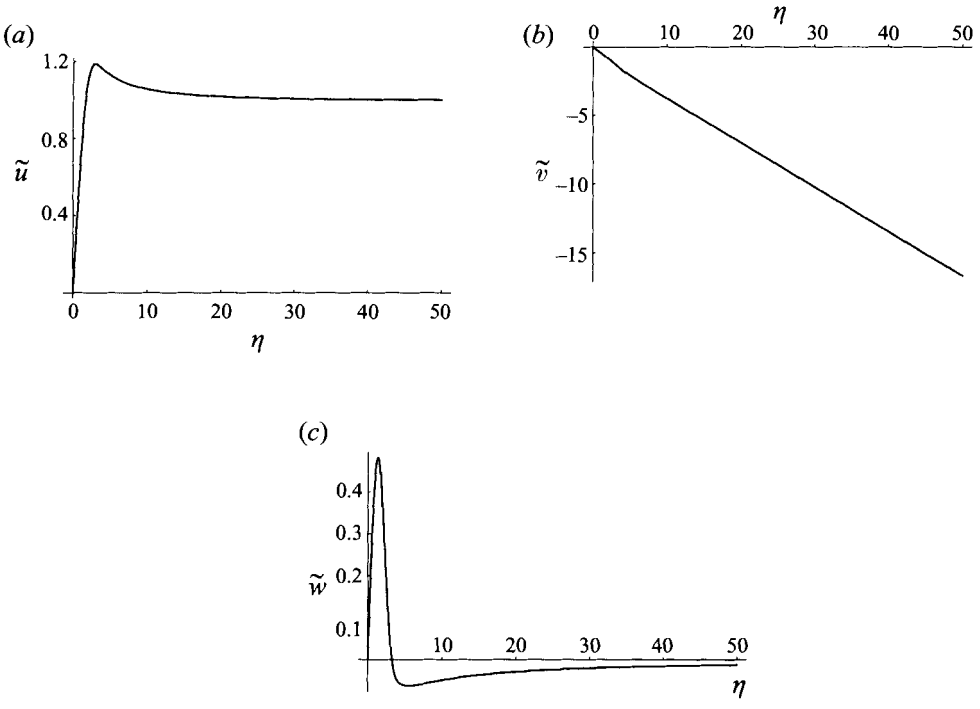

FIGURE 3. (*a*) The streamwise velocity component $\tilde{u}(\eta)$, (*b*) the normal velocity component $\tilde{v}(\eta)$, (*c*) the azimuthal velocity component $\tilde{w}(\eta)$, calculated from the numerical solution of the interactive version of (4.20).

currently beyond the computing resources at our disposal. The lack of resolution can be seen clearly in figure 5(*e*) where the energies

$$e_n(\tilde{x}) = \int_0^\infty U_n U_n^* + W_n W_n^* \, \mathrm{d}\tilde{Y}, \tag{4.21}$$

for $n = 1, 2, 3$ are displayed, with mode 2 becoming dominant as $\tilde{x}$ increases. The computations suggest that the interaction affects the flow significantly over a relatively short streamwise lengthscale. In addition the major activity appears to be concentrated close to the pipe wall which suggests that in future computations mesh points should be concentrated in this region rather than being spread uniformly as is currently the case.

5. Starting solutions for the wide vortex–TS interaction

In this section we postulate how the wide vortex-TS interaction formulated in §§2 and 3 develops spatially from an initially two-dimensional boundary layer upon the introduction of a three-dimensional neutral TS wave. The behaviour in the three regions I, II*a* and II*b* is discussed in turn. The analysis concentrates entirely on the case of spatial evolution of the vortex flow, i.e. we take $\partial/\partial\bar{t} \equiv 0$ in (2.16) and (3.7). In addition to being of interest in its own right, this study also provides suitable starting conditions for a full numerical solution of the interaction equations.

We assume that the wave has a starting amplitude proportional to

$$Q\cos\beta\bar{\theta}. \tag{5.1}$$

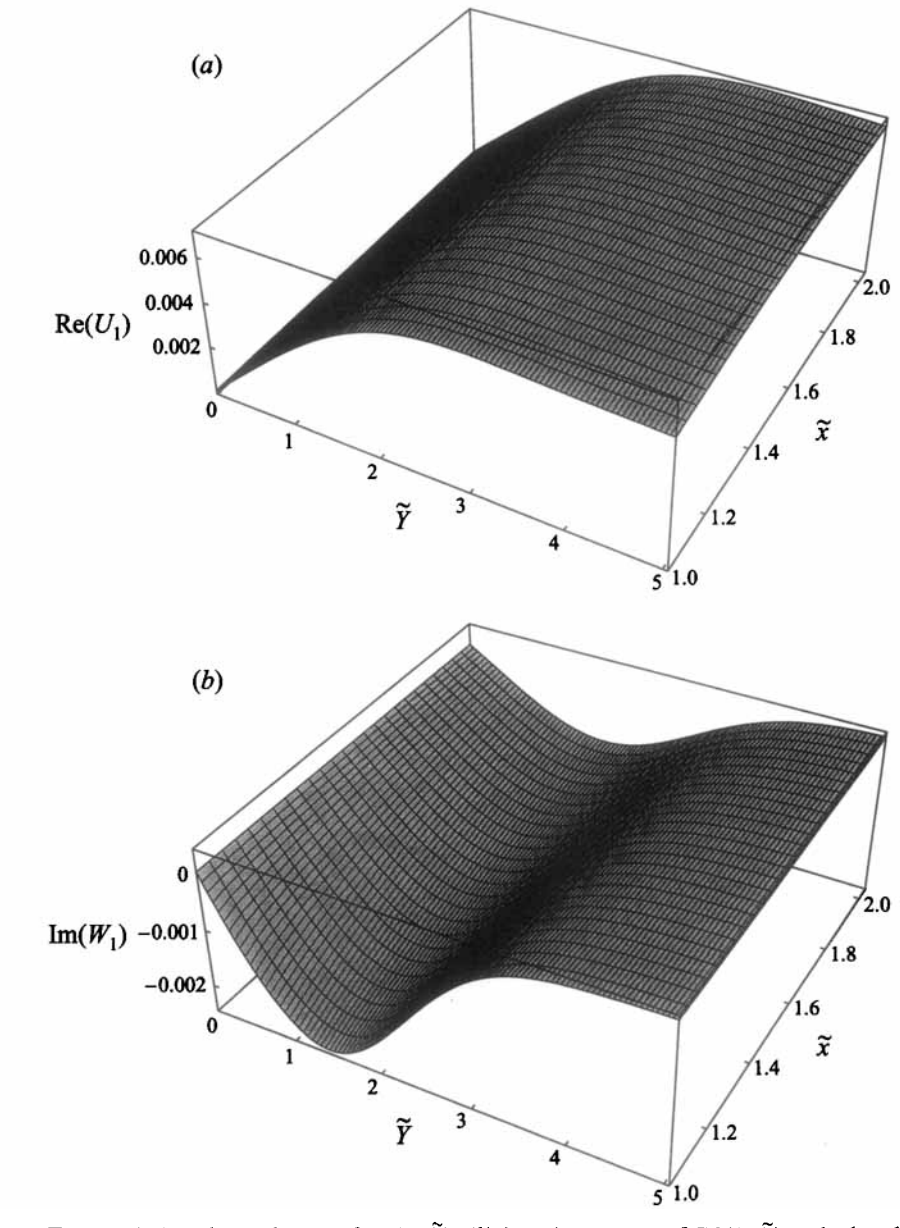

FIGURE 4. (*a*) The real part of $U_1(\tilde{x}, \tilde{Y})$, (*b*) imaginary part of $W_1(\tilde{x}, \tilde{Y})$, calculated from the numerical solution of the non-interactive version of (4.12).

In region I, the spanwise wavenumber β is a real parameter, while for a wave input in regions II*a* and II*b* we require $\beta = N$, an integer, in view of the $O(1)$ azimuthal scaling in these regions. The main result from this analysis will be the determination of the modulus of the complex quantity Q as a function of β or N. We take the undisturbed boundary layer to be of the Blasius form since this is an exact solution of (2.16) with $U_e \equiv 1$ (or of (3.7)). Thus at the streamwise location $\bar{x} = x_0$ we suppose:

$$U_0 = f'_B(\eta), \quad V_0 = \tfrac{1}{2}x_0^{-1/2}(\eta f'_B - f_B), \quad W_0 = 0, \tag{5.2}$$

with $\eta = \bar{Y}/x_0^{1/2}$. Initially, the main effects of the wave on the mean flow are confined near to the wall in a sublayer of thickness $O(\bar{x}-x_0)^{1/3}$ relative to the boundary layer.

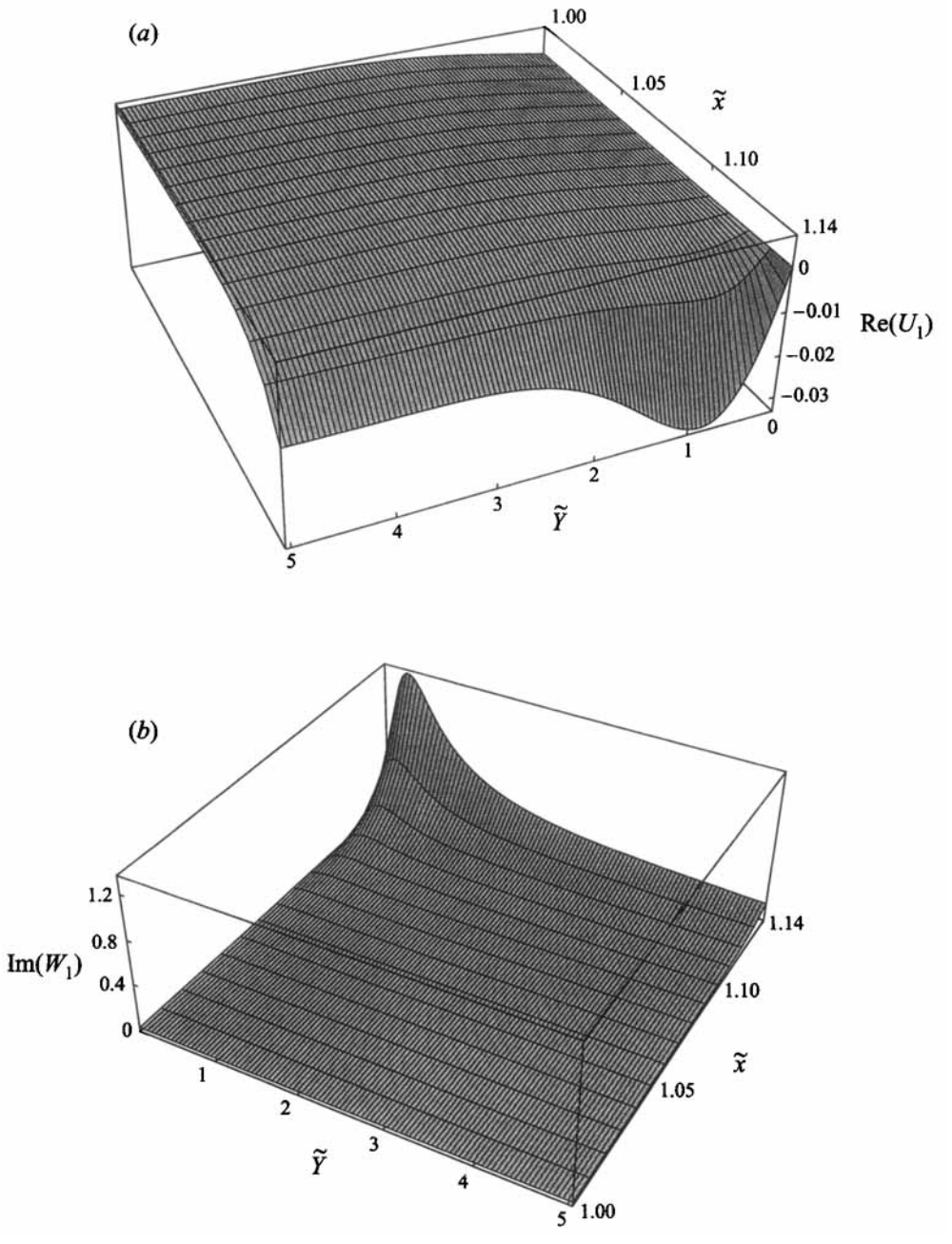

FIGURE 5(a, b). For caption see facing page.

In this region the flow expands in the form

$$U_0 = (\bar{x}-x_0)^{1/3}\frac{\hat{\lambda}\xi}{x_0^{1/2}} + (\bar{x}-x_0)^{4/3}\left(-\frac{1}{2}\frac{\hat{\lambda}\xi}{x_0^{3/2}} + \frac{\lambda_4\xi^4}{x_0^2} + 2\beta u_1(\xi)\cos 2\beta\bar{\theta}\right) + \ldots, \quad (5.3a)$$

$$V_0 = (\bar{x}-x_0)^{2/3}\left(\frac{1}{4}\frac{\hat{\lambda}\xi^2}{x_0^{3/2}} + 2\beta v_1(\xi)\cos 2\beta\bar{\theta}\right) + \ldots, \quad (5.3b)$$

$$W_0 = (\bar{x}-x_0)^{1/3} w_1(\xi)\sin 2\beta\bar{\theta} + \ldots, \quad (5.3c)$$

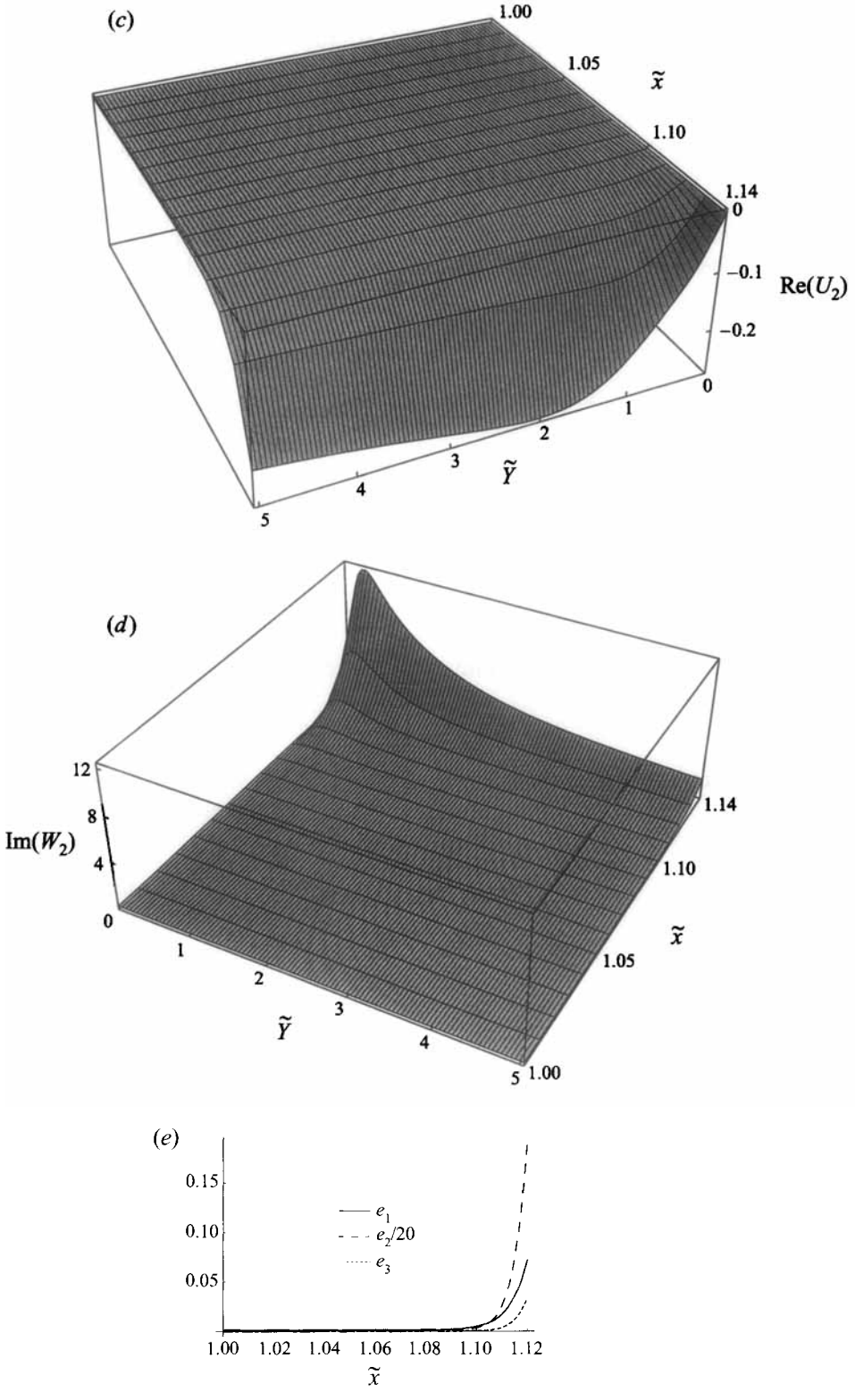

FIGURE 5. (*a*) The real part of $U_1(\tilde{x}, \tilde{Y})$, (*b*) imaginary part of $W_1(\tilde{x}, \tilde{Y})$, (*c*) real part of $U_2(\tilde{x}, \tilde{Y})$, (*d*) imaginary part of $W_2(\tilde{x}, \tilde{Y})$, (*e*) the energies associated with modes 1–3, calculated from the numerical solution of the interactive version of (4.12).

where $\bar{Y} = (\bar{x}-x_0)^{1/3}\xi$. Here, the terms independent of $\bar{\theta}$ arise from the Taylor expansion of the near-wall form for the Blasius solution about the point $\bar{x} = x_0$, with $\hat{\lambda} \simeq 0.33205$, $\lambda_4 = -\hat{\lambda}^2/48$. The powers of $(\bar{x}-x_0)$ in (5.3) are determined by the following two requirements: (i) the terms (u_1, v_1, w_1) representing the effects of the wave on the mean flow should be of the same magnitude as the non-parallel corrections to the Blasius flow; (ii) the thickness of the region should be such that the behaviour of the wave terms is governed by viscous effects at leading order. The dependence in (5.3) on the second harmonic is forced by the form (5.1) for the TS wave via the azimuthal forcing, i.e. equations (3.7*d*) and (3.7*f*); we will return to this point later. Substitution of (5.3) into either (2.16*a–c*) or (3.7*a–c*) leaves (u_1, v_1, w_1) controlled by

$$\tfrac{4}{3}u_1 - \tfrac{1}{3}\xi u_1' + v_1' + w_1 = 0, \tag{5.4a}$$

$$\frac{\hat{\lambda}}{x_0^{1/2}}(\tfrac{4}{3}\xi u_1 - \tfrac{1}{3}\xi^2 u_1' + v_1) = u_1'', \tag{5.4b}$$

$$\frac{\hat{\lambda}}{x_0^{1/2}}(\tfrac{1}{3}\xi w_1 - \tfrac{1}{3}\xi^2 w_1') = w_1''. \tag{5.4c}$$

The relevant outer boundary conditions are:

$$w_1 \to 0, \quad u_1' \to 0 \quad \text{as} \quad \xi \to \infty, \tag{5.4d}$$

ensuring that the main three-dimensional effects are confined to the sublayer. The lower conditions are:

$$u_1 = v_1 = 0, \quad w = -\hat{q} \quad \text{on} \quad \xi = 0, \tag{5.4e}$$

where the wave-induced azimuthal slip velocity $\hat{q}$ will be calculated presently from (3.7*f*). Before attempting to solve (5.4) it is convenient to rescale the variables to remove the constants $\hat{\lambda}$ and $\hat{q}$. Thus we write

$$u_1 = -\hat{q}\hat{u}_1(\hat{\xi}), \quad v_1 = -\hat{q}\hat{v}_1(\hat{\xi}), \quad w_1 = -\hat{q}\hat{w}_1(\hat{\xi}), \quad \hat{\xi} = (\hat{\lambda}/x_0^{1/2})^{1/3}\xi. \tag{5.5}$$

Under this rescaling, (5.4) become

$$\tfrac{4}{3}\hat{u}_1 - \tfrac{1}{3}\hat{\xi}\hat{u}_1' + \hat{v}_1' + \hat{w}_1 = 0, \tag{5.6a}$$

$$\tfrac{4}{3}\hat{\xi}\hat{u}_1 - \tfrac{1}{3}\hat{\xi}^2\hat{u}_1' + \hat{v}_1 = \hat{u}_1'', \tag{5.6b}$$

$$\tfrac{1}{3}\hat{\xi}\hat{w}_1 - \tfrac{1}{3}\hat{\xi}^2\hat{w}_1' = \hat{w}_1''. \tag{5.6c}$$

$$\hat{u}_1(0) = \hat{v}_1(0) = 0, \quad \hat{w}_1(0) = 1, \quad \hat{u}_1'(\infty) = \hat{w}_1(\infty) = 0. \tag{5.6d–f}$$

Plots of the behaviour of $\hat{u}_1$, $\hat{v}_1$ and $\hat{w}_1$ from the numerical solution of (5.6) are shown in figures 6(*a*)–6(*c*). For the present calculation concerning the determination of the wave amplitude Q, the quantity of interest from this solution is

$$\hat{u}_1'(0) = \frac{\Gamma(\frac{2}{3})}{3^{2/3}} \simeq 0.650992. \tag{5.7}$$

Recall that the azimuthal slip velocity and the wave pressure are linked via the relation

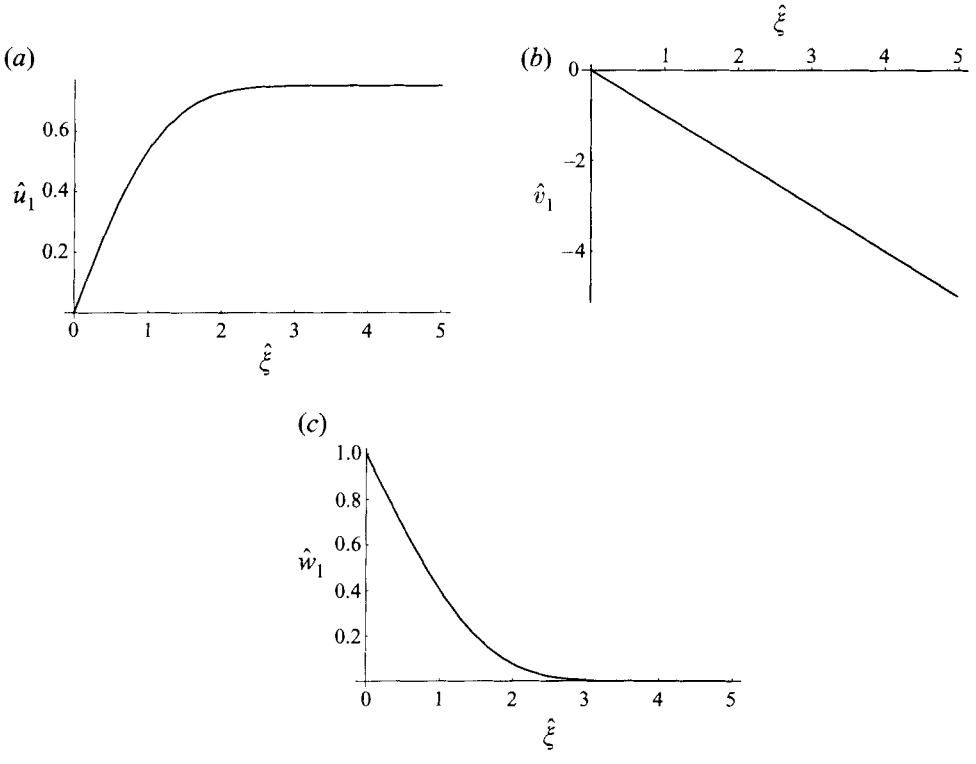

FIGURE 6. (*a*) the streamwise velocity component $\hat{u}_1(\hat{\xi})$, (*b*) the normal velocity component $\hat{v}_1(\hat{\xi})$, (*c*) the azimuthal velocity component $\hat{w}_1(\hat{\xi})$, calculated from the numerical solution of (5.6).

$$W_0 = -\frac{1}{\alpha^2\lambda^2}\frac{\partial}{\partial\bar{\theta}}\left\{\alpha^2 p_{11}p_{11}^* + \frac{\partial p_{11}}{\partial\bar{\theta}}\frac{\partial p_{11}^*}{\partial\bar{\theta}}\right\} \quad \text{on} \quad \bar{Y}=0, \tag{5.8}$$

from (3.7*d*, *f*). From (5.3) and (5.5), the skin-friction λ present in (5.8) is of the form

$$\lambda = (\bar{x}-x_0)^{-1/3}\left.\frac{\partial U_0}{\partial\xi}\right|_{\xi=0}$$

$$= \frac{\hat{\lambda}}{x_0^{1/2}}\left[1+(\bar{x}-x_0)\left(-\frac{1}{2x_0}-2\beta\hat{q}\left(\frac{\hat{\lambda}}{x_0^{1/2}}\right)^{-2/3}\hat{u}_1'(0)\cos 2\beta\bar{\theta}\right)+\ldots\right]. \tag{5.9}$$

Thus, upon assuming an initial development for the wave of the form

$$p_{11} = (\bar{x}-x_0)^{1/6}(Q\cos\beta\bar{\theta}+(\bar{x}-x_0)p_1(\bar{\theta})+\ldots), \tag{5.10}$$

with wavenumber

$$\alpha = \alpha_0(1+(\bar{x}-x_0)\alpha_1+\ldots), \tag{5.11}$$

we deduce from (5.3*c*), (5.4*e*), (5.8) and (5.9) that the slip velocity is given in terms of the wave amplitude by

$$\hat{q} = \frac{\beta(\beta^2-\alpha_0^2)}{\alpha_0^2(\hat{\lambda}^2/x_0)}|Q|^2. \tag{5.12}$$

Using (5.12), the skin-friction distribution of (5.9) can be written in the form

$$\lambda = \frac{\hat{\lambda}}{x_0^{1/2}}\left[1+(\bar{x}-x_0)\left(-\frac{1}{2x_0}+\lambda_{11}\cos 2\beta\bar{\theta}\right)+\ldots\right], \tag{5.13}$$

where

$$\lambda_{11} = \frac{2\beta^2}{\alpha_0^2}(\alpha_0^2-\beta^2)\left(\frac{\hat{\lambda}}{x_0^{1/2}}\right)^{-8/3}\hat{u}_1'(0)\,|Q|^2.$$

To determine the quantity $|Q|^2$, we substitute the expansions (5.10), (5.11) and (5.13) into the pressure equation (3.7g) and compare like powers of $(\bar{x}-x_0)$. To achieve consistency with (5.10), we expand the wave displacement A_{11} in the form

$$A_{11} = (\bar{x}-x_0)^{1/6}(A_0\cos\beta\bar{\theta}+(\bar{x}-x_0)\,A_1+\ldots), \tag{5.14}$$

with the behaviour of A_0, A_1 governed by (2.18) in region I and by (3.7h) in regions IIa and IIb. At $O(1)$ in (3.7g), we obtain the linear eigenrelation for the TS waves, relating the streamwise wavenumber α_0 to the azimuthal wavenumber β (or N) and the distance downstream x_0. In region I, where the flow is effectively an external one, this has the form

$$\alpha_0^{1/3}(\beta^2+\alpha_0^2)^{1/2} = (\hat{\lambda}/x_0^{1/2})^{5/3}\,d_1 \quad (d_1 \simeq 1.00065), \tag{5.15}$$

whilst in region IIa we have

$$N^2+\alpha_0^2 = \alpha_0^{2/3}(\hat{\lambda}/x_0^{1/2})^{5/3}d_1\frac{I_N'(\alpha_0)}{I_N(\alpha_0)}. \tag{5.16}$$

Finally, further downstream in region IIb, the eigenrelation reduces to

$$N = \alpha_0^{-1/3}(\hat{\lambda}/x_0^{1/2})^{5/3}d_1. \tag{5.17}$$

As expected, these relations match to each other in the appropriate limits. For example, starting with (5.16), equation (5.15) is obtained in the upstream limit α_0, $N\to\infty$, while (5.17) is obtained in the downstream limit $\alpha_0\to 0$. At $O(\bar{x}-x_0)$ in the wave pressure equation (3.7g), comparing coefficients of $\cos\beta\bar{\theta}$, we deduce the equation

$$\omega_1\alpha_1+\omega_2|Q|^2+\omega_3 = 0, \tag{5.18}$$

relating the amplitude Q to the wavenumber correction α_1, where ω_1, ω_2 and ω_3 are complex constants. The solution for $|Q|^2$ is then

$$|Q|^2 = \frac{\omega_{3i}\omega_{1r}-\omega_{3r}\omega_{1i}}{\omega_{2r}\omega_{1i}-\omega_{2i}\omega_{1r}}. \tag{5.19}$$

Although the form of (5.19) is the same in all three regions the coefficients are different in view of the difference in the eigenrelations (5.15)–(5.17). In view of the fact that in regions I and IIb, the input location L has been scaled out of the problem via (3.3)–(3.6) and (3.11)–(3.16), respectively, we can take $x_0 = 1$ without loss of generality. In the adjustment region IIa however, x_0 is allowed to vary (in effect, $L\equiv x_0$ in this region). We expect to match IIa with the upstream region I as $x_0\to 0$ and with the downstream region IIb as $x_0\to\infty$. In region I the coefficients ω_1, ω_2 and ω_3 have the form:

$$\omega_1 = -3\alpha_0^2-2\beta^2-\alpha_0^{-1/3}(\beta^2+\alpha_0^2)^{1/2}(\hat{\lambda}/x_0^{1/2})^{5/3}\hat{\chi}, \tag{5.20a}$$

$$\omega_2 = -\frac{2\beta^2(\alpha_0^2-\beta^2)\,\hat{u}_1'(0)}{\alpha_0^2(\hat{\lambda}/x_0^{1/2})^{8/3}}\left[\beta^2\mathscr{F}_0+\frac{(\beta^2+\alpha_0^2)^{1/2}\hat{\chi}}{2\alpha_0^{1/3}}\right], \tag{5.20b}$$

$$\omega_3 = \frac{(\beta^2+\alpha_0^2)^{1/2}\hat{\chi}}{2x_0\alpha_0^{1/3}}; \tag{5.20c}$$

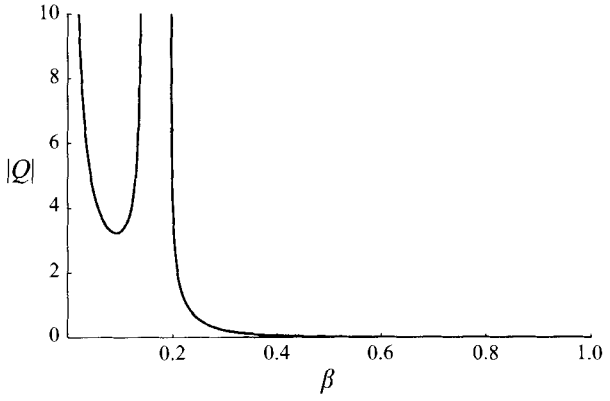

FIGURE 7. Region I: $|Q|$ versus azimuthal wavenumber β.

in region IIa:

$$\omega_1 = -2\alpha_0^2 + (N^2+\alpha_0^2)\left[-2 + \frac{(N^2+\alpha_0^2)}{\alpha_0}\frac{I_N(\alpha_0)}{I_N'(\alpha_0)} - \alpha_0\frac{I_N'(\alpha_0)}{I_N(\alpha_0)}\right] - \alpha_0^{2/3}\frac{I_N'(\alpha_0)}{I_N(\alpha_0)}(\hat{\lambda}/x_0^{1/2})^{5/3}\hat{\chi}, \tag{5.21a}$$

$$\omega_2 = -\frac{2N^2(\alpha_0^2-N^2)\hat{u}_1'(0)}{\alpha_0^2(\hat{\lambda}/x_0^{1/2})^{8/3}}\left[N^2\mathscr{F}_0 + \tfrac{1}{2}\alpha_0^{2/3}\frac{I_N'(\alpha_0)}{I_N(\alpha_0)}(\hat{\lambda}/x_0^{1/2})^{5/3}\hat{\chi}\right], \tag{5.21b}$$

$$\omega_3 = \frac{1}{2x_0}\alpha_0^{2/3}\frac{I_N'(\alpha_0)}{I_N(\alpha_0)}(\hat{\lambda}/x_0^{1/2})^{5/3}\hat{\chi} \tag{5.21c}$$

and in region IIb:

$$\omega_1 = -2N^2 - \alpha_0^{-1/3}N(\hat{\lambda}/x_0^{1/2})^{5/3}\hat{\chi}, \tag{5.22a}$$

$$\omega_2 = \frac{2N^4\hat{u}_1'(0)}{\alpha_0^2(\hat{\lambda}/x_0^{1/2})^{8/3}}(N^2\mathscr{F}_0 + \tfrac{1}{2}\alpha_0^{-1/3}N(\hat{\lambda}/x_0^{1/2})^{5/3}\hat{\chi}), \tag{5.22b}$$

$$\omega_3 = \frac{1}{2x_0}\alpha_0^{-1/3}N(\hat{\lambda}/x_0^{1/2})^{5/3}\hat{\chi}. \tag{5.22c}$$

In (5.20)–(5.22) the complex constants $\hat{\chi}$ and $\mathscr{F}_0$ are given approximately by

$$\hat{\chi} \simeq -0.5854 - 0.8122\mathrm{i}, \quad \mathscr{F}_0 \simeq 0.1884 + 1.7480\mathrm{i}. \tag{5.23}$$

Although we have referred to $|Q|$ as an amplitude above, we see from (5.10) that the wave starts from zero amplitude with $|Q|$ representing a measure of how rapidly the wave develops. For large values of $|Q|$ the interaction can only be described by linear theory for short distances from the location of wave input. In a controlled experiment it may be possible to realize these starting conditions by placing a vibrating ribbon in the neighbourhood of the lower branch neutral point.

We now discuss the solutions given by (5.19) in each of the regions in turn. We begin with figure 7 where we have plotted $|Q|$ versus azimuthal wavenumber β. The plot is obtained from the solution of (5.15), (5.19) and (5.20) with $x_0 = 1$ and is similar to that obtained by Walton, Bowles & Smith (1994) for a VWI near separation. There are a range of azimuthal wavenumbers for which no VWI solutions are possible. This is due to the fact that the denominator of (5.19) is negative in this range while the

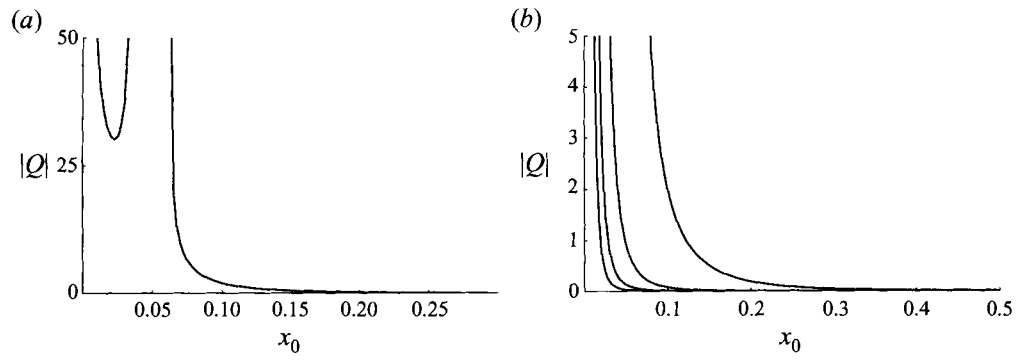

FIGURE 8. Region IIa: (a) $|Q|$ versus distance x_0 for azimuthal wavenumber $N = 1$; (b) $|Q|$ versus x_0 for $N = 1, 2, 3, 4$ (from right to left).

numerator remains positive. It can be shown that the two associated singular locations β_{c1}, β_{c2} occur when

$$\beta_{c1} \simeq 0.630\alpha_0, \quad \beta_{c2} = \alpha_0.$$

Substituting into (5.15) we deduce

$$\beta_{c1} \simeq 0.140, \quad \beta_{c2} \simeq 0.195.$$

It is clear that $|Q|$ is also singular at $\beta = 0$. The scaling (3.3) indicates that the effective azimuthal wavenumber decreases like $L^{-5/8}$ as $L \to O(1)$. Thus, starting the interaction further downstream corresponds to moving to the left on figure 7. At the downstream end of region I, therefore, the appropriate value of $|Q|$ is large, since $|Q| \propto 1/\beta$ as $\beta \to 0$. We conclude that in this region the interaction develops rapidly. It seems plausible that an interaction initiated with $\beta < \beta_{c1}$ will evolve downstream into region II in the manner predicted by the scalings of §3. If the interaction is started on the right-hand branch of figure 7, however, it is impossible on the basis of this linear theory for β to reach zero. This suggests that such interactions will terminate in a finite-distance singularity within region I. This possibility is consistent with the results of Walton, Bowles & Smith (1994) who found that such singularities arose when integrating numerically a simplified version of the wide vortex, starting from a similar location in their version of figure 7.

As the input location is moved further downstream, the required azimuthal scaling for the TS wave eventually increases to $O(1)$ and region IIa is entered. In figure 8 we present the solution for $|Q|$, calculated from (5.16), (5.19) and (5.21). Figure 8(a) shows the variation of $|Q|$ with input location x_0 for azimuthal wavenumber $N = 1$. We see that there are no solutions possible in a small region near the beginning of IIa: for larger wavenumbers this region disappears. It is evident that $|Q|$ falls rapidly with distance. In other words, the interaction develops more slowly the further downstream the input location. This is not unreasonable since the basic flow is developing internal properties and becoming more stable. In figure 8(b) we show $|Q|$ versus x_0 on a different scale for $N = 1, 2, 3, 4$. For all values of N it can be shown that $|Q| \propto x_0^{-1/2}$ as $x_0 \to 0$. In this limit, with N large, matching is achieved with the small-β solutions of region I. In the downstream limit $x_0 \to \infty$, a match is achieved to region IIb. Table 1 presents the values of $|Q|$ for $N = 1, 2, 3, 4, 5$ for the solution in IIb, calculated from (5.17), (5.19) and (5.22) with $x_0 = 1$. The values of $|Q|$ are extremely small and decrease rapidly with increasing N. The solutions also decrease with increasing L, in view of the pressure scaling (3.13d). Nevertheless, an interaction can still be initiated in this region; whether

N	$\|Q\|$
1	0.0005451
2	0.0000170
3	0.0000022
4	0.0000005
5	0.0000002

TABLE 1. Region IIb: $|Q|$ *vs.* N for $N = 1, 2, 3, 4, 5$.

such an interaction will persist can only be determined by a full numerical solution of the governing equations (3.7).

In summary, the wide vortex VWI can evolve from an initially two-dimensional Blasius boundary layer in each of the three regions I, IIa and IIb. The interaction develops more rapidly in region I with TS waves possessing a short spanwise scaling appearing particularly dangerous. In regions IIa and IIb, by contrast, it is the $N = 1$ mode which develops most rapidly. In general, the VWI develops more slowly as the input location is moved downstream.

The starting form proposed here becomes invalid very close to the position of wave input. The lengthscale associated with this inner region can be determined by balancing the order of magnitude of the correction to the wavelength of the TS wave, $L^{5/8}(\bar{x}-x_0)^{-1}$ from (3.3) and (5.11), with the lengthscale over which the mean flow is developing ($\epsilon^{-3}L(\bar{x}-x_0)$). This gives a shortened lengthscale $R^{-3/10}L^{-3/16}\hat{x}$ with $\hat{x}$ of $O(1)$, over which it can be shown that the pressure amplitude satisfies a nonlinear integro-differential equation of the form

$$\frac{\mathrm{d}}{\mathrm{d}\hat{x}}|p_{11}|+\left(-K_1\hat{x}+K_2\int_{-a}^{\hat{x}}|p_{11}(s)|^2(\hat{x}-s)^{-1/3}\,\mathrm{d}s\right)|p_{11}| = 0, \tag{5.24}$$

where $-a$ denotes a wave input location slightly upstream of the neutral point. On this lengthscale the VWI is of the weakly nonlinear form studied by Hall & Smith (1989), Blackaby (1994), among others. In the case of interest here the constants K_1, K_2 are positive with $K_1/K_2 = Q^2$. Numerical calculations performed by Blackaby (1994) for relatively arbitrary wave input at $\hat{x} = -a$ show that the solution grows algebraically with $p_{11} \sim \hat{x}^{1/6}Q$ as $\hat{x} \to \infty$, which provides an exact match to the similarity solution presented above. Thus, it would appear that a weak interaction occurs close to the neutral point, naturally promoting the amplitude of the wave to the required size for the strong interaction to take over on the longer lengthscale. Incidentally, the range of azimuthal wavenumbers for which no strong interaction is possible corresponds to the case of $K_2 < 0$ and the occurrence of a finite-distance singularity in the numerical solution of (5.24). A similar analysis may be performed for the small vortex of §4 with the buffer layer acquiring the similarity solution studied in Walton & Smith (1992).

6. Discussion

In this paper we have presented the governing equations describing two types of strong vortex–TS interaction. In both cases, it is possible to obtain scalings with respect to downstream distance $\hat{L}$ that ensure that the form of the interaction equations remains relatively unchanged as $\hat{L}$ is increased. At a distance of $O(R^{3/5})$ there is an adjustment region (IIa) beyond which the flow develops internal characteristics. An interesting result is that the small vortex, which involves larger disturbances than the

wide vortex, develops in an analogous fashion until a distance of order $R^{3/5}/h^2 \ll O(R)$, when the wave and induced mean flow lengthscales become comparable. Numerical solutions of the resulting three-dimensional triple-deck problem indicate that the flow acquires a complicated three-dimensional character as it develops downstream, with the major activity confined close to the pipe wall. The solutions presented here are time-independent: an obvious next step is to carry out an unsteady numerical calculation and try and compare the results with those arising from largescale numerical simulations.

A significant result from the analysis of §5 is that in all regions of the pipe with $\hat{L} < O(R)$, the wide vortex–TS interaction can be initiated from a two-dimensional boundary layer, with a three-dimensional neutral TS wave being amplified initially via a weak interaction on a short lengthscale about the neutral point, followed by the stronger interaction on a longer lengthscale. This is in contrast to the vortex–Rayleigh wave interaction where it appears that such a natural amplification is the exception rather than the norm, (Brown *et al.* 1993). In view of this, efforts should be made in the future to obtain numerical solutions of the governing equations using starting conditions of the form investigated in §5.

The author wishes to thank Professor F. T. Smith for suggesting the original problem and for many useful discussions concerning various aspects of the work, and to the referees for their comments on an earlier version of the paper.

REFERENCES

BLACKABY, N. D. 1994 Tollmien–Schlichting/vortex interactions in compressible boundary layer flows. *IMA J. Appl. Maths* **53**, 191–214.

BROWN, P. G., BROWN, S. N., SMITH, F. T. & TIMOSHIN, S. N. 1993 On the starting process of strongly nonlinear vortex/Rayleigh–wave interactions. *Mathematika* **40**, 7–29.

CORCOS, G. M. & SELLARS, J. R. 1959 On the stability of fully developed flow in a pipe. *J. Fluid Mech.* **5**, 97–112.

COWLEY, S. J. & WU, X. 1994 Asymptotic approaches to transition modelling. In *Progress in Transition Modelling. AGARD Rep.* 793, pp. 1–38.

CRABTREE, L. F., KÜCHEMANN, D. & SOWERBY, L. 1963 Three-dimensional boundary layers. In *Laminar Boundary Layers* (ed. L. Rosenhead), pp. 409–491. Dover.

DAVEY, A. & DRAZIN, P. G. 1969 The stability of Poiseuille flow in a pipe. *J. Fluid Mech.* **36**, 209–218.

FLETCHER, C. A. J. 1991 *Computational Techniques for Fluid Dynamics*, vol. 2. Springer.

GARG, V. K. & ROULEAU, W. T. 1972 Linear spatial stability of pipe Poiseuille flow. *J. Fluid Mech.* **54**, 113–127.

GILL, A. E. 1965 On the behaviour of small disturbances to Poiseuille flow in a circular pipe. *J. Fluid Mech.* **21**, 145–172.

HALL, P. & SMITH, F. T. 1988 The nonlinear interaction of Tollmien–Schlichting waves and Taylor–Görtler vortices in curved channel flows. *Proc. R. Soc. Lond.* A **417**, 255–282.

HALL, P. & SMITH, F. T. 1989 Nonlinear Tollmien–Schlichting/vortex interaction in boundary layers. *Eur. J. Mech.* B **8**, 179–205.

HALL, P. & SMITH, F. T. 1991 On strongly nonlinear vortex/Wave interactions in boundary-transition. *J. Fluid Mech.* **227**, 641–666.

HOYLE, J. M. & SMITH, F. T. 1994 On finite-time break-up in three-dimensional unsteady interactive boundary layers. *Proc. R. Soc. Lond.* A **447**, 467–492.

REYNOLDS, O. 1883 An experimental investigation of the circumstances which determine whether the motion of water will be direct or sinuous, and of the law of resistance in parallel channels. *Phil. Trans. R. Soc. Lond.* A **174**, 935–982.

SMITH, F. T. 1979*a* On the non-parallel flow stability of the Blasius boundary layer. *Proc. R. Soc. Lond.* A **366**, 91–109.

SMITH, F. T. 1979*b* Instability of flow through pipes of general cross-section, part 1. *Mathematika* **26**, 187–210.

SMITH, F. T. & BLENNERHASSETT, P. 1992 Nonlinear interaction of oblique three-dimensional Tollmien–Schlichting waves and longitudinal vortices in channel flows and boundary layers. *Proc. R. Soc. Lond.* A **436**, 585–602.

SMITH, F. T. & BODONYI, R. J. 1980 On the stability of the developing flow in a channel or circular pipe. *Q. J. Mech. Appl. Maths* **33**, 293–320.

SMITH, F. T. & WALTON, A. G. 1989 Nonlinear interaction of near-planar TS waves and longitudinal vortices in boundary-layer transition. *Mathematika* **36**, 262–289.

WALTON, A. G. 1991 Theory and computation of three-dimensional nonlinear effects in pipe flow transition. PhD thesis, University of London.

WALTON, A. G., BOWLES, R. I. & SMITH, F. T. 1994 Vortex-wave interaction in separating flows. *Eur. J. Mech.* B **13**, 629–655.

WALTON, A. G. & SMITH, F. T. 1992 Properties of strongly nonlinear vortex/Tollmien–Schlichting-wave interactions. *J. Fluid Mech.* **244**, 649–676.

WYGNANSKI, I. J. & CHAMPAGNE, F. H. 1973 On transition in a pipe. Part 1. The origin of puffs and slugs and the flow in a turbulent slug. *J. Fluid Mech.* **59**, 281–335.